Synthetic-Aperture Radar (SAR) Image Formation Processing

Outline

- Raw SAR image characteristics
- Algorithm basics
  - Range compression
  - Range cell migration correction
  - Azimuth compression
  - Motion compensation
- Types of algorithms
  - Range Doppler algorithm
  - Chirp scaling algorithm
  - Frequency-wavenumber algorithm (ω-k or f-k)
- Comparison of algorithms
  - Processing errors, Computational load, Pros and cons
- Autofocus techniques

Airborne SAR real-time IFP block diagram

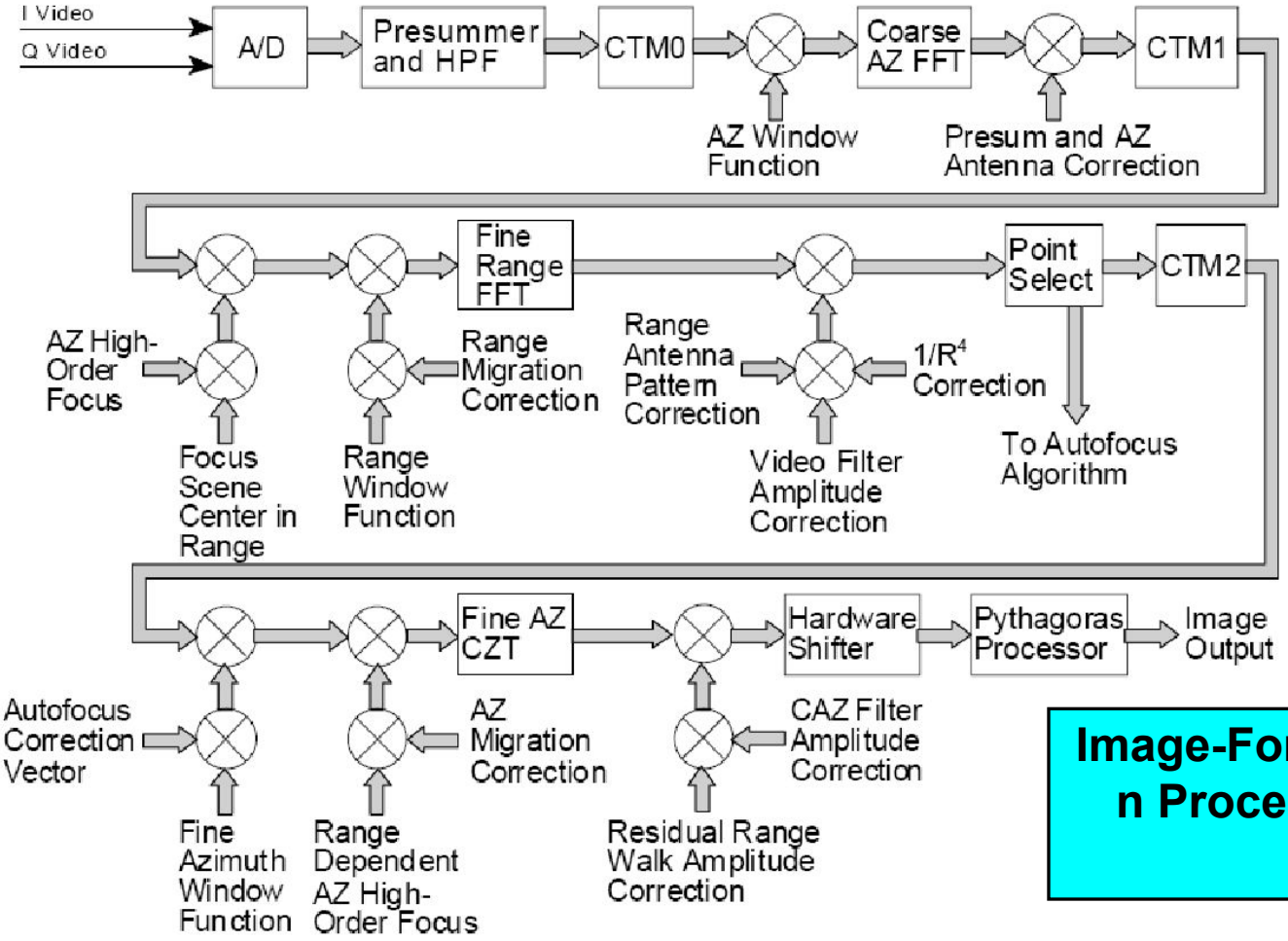

Figure 7. Functional Diagram of Overlapped Subaperture Algorithm

New terminology:
Presum (a.k.a. coherent integration)
Corner-turning memory (CTM)
Window Function

Focus and Correction Vectors
Range Migration and Range Walk
Fast Fourier transform (FFT)
Chirp-z transform (CZT)

Basic SAR image formation processes

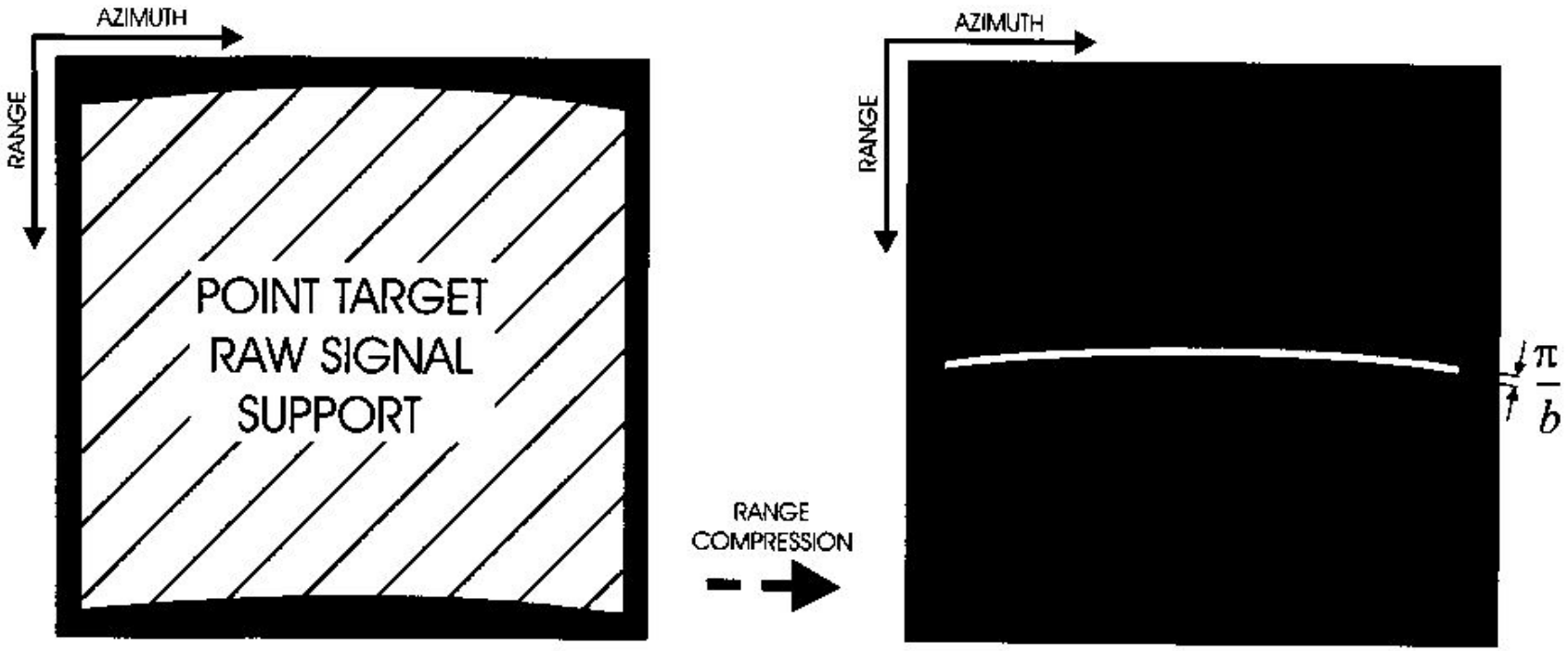

FIGURE 1A Point target located over an absorbing background. Range compression; normalized range resolution is given by π/b.

Basic SAR image formation processes

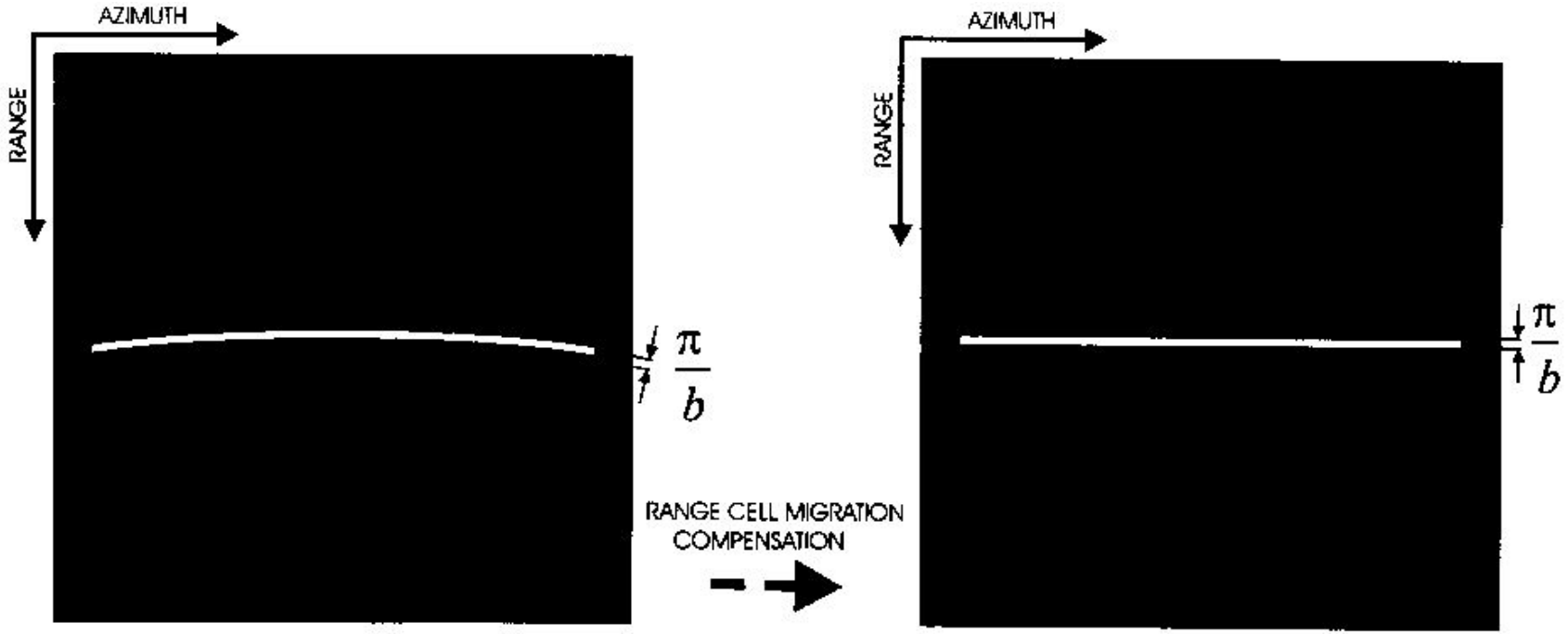

FIGURE 1B Same as Figure 1A. Range cell migration compensation.

Basic SAR image formation processes

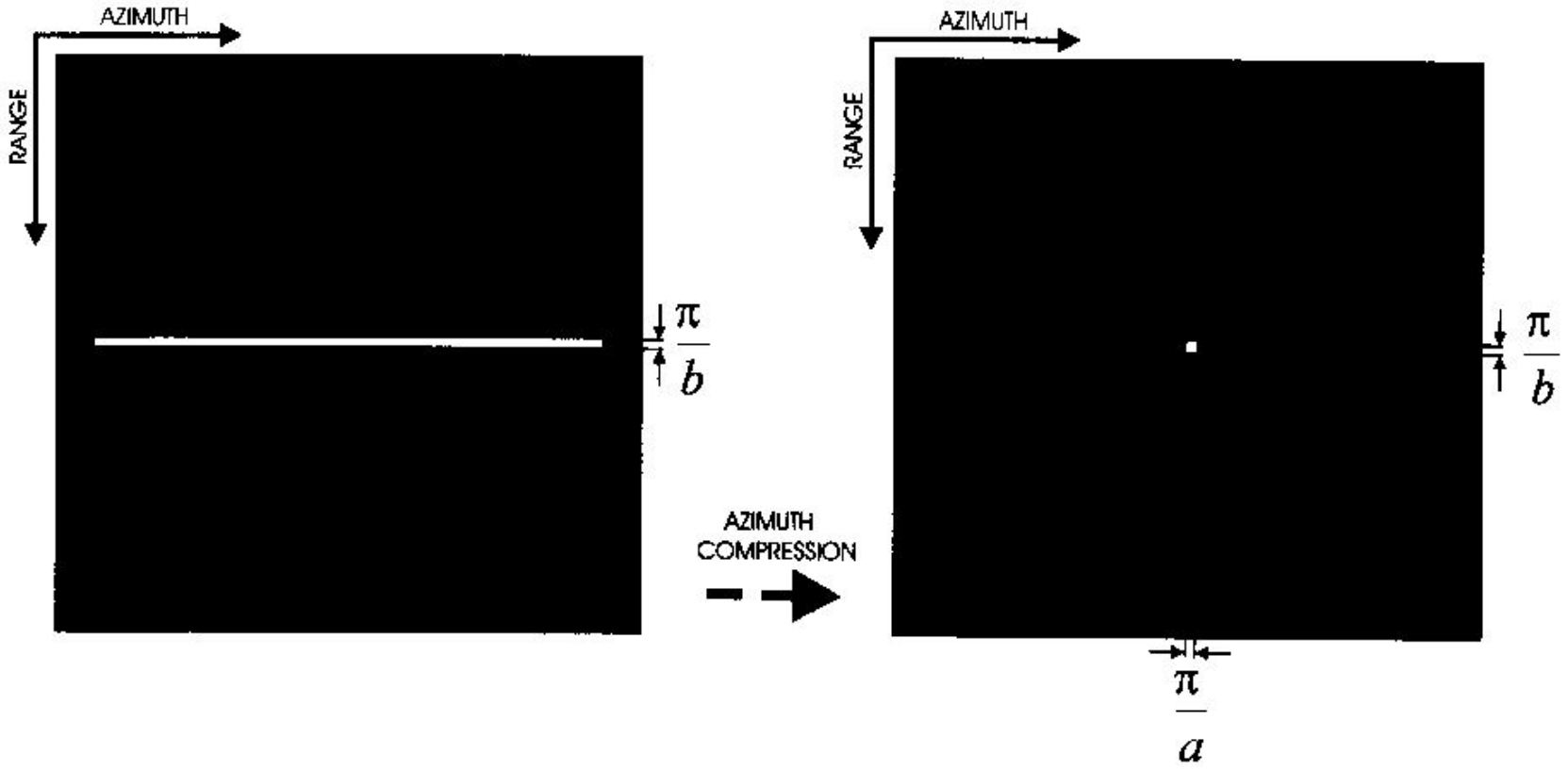

FIGURE 1C Same as Figure 1A. Azimuth compression; normalized azimuth resolution is given by π/a.

Basic SAR image formation processes

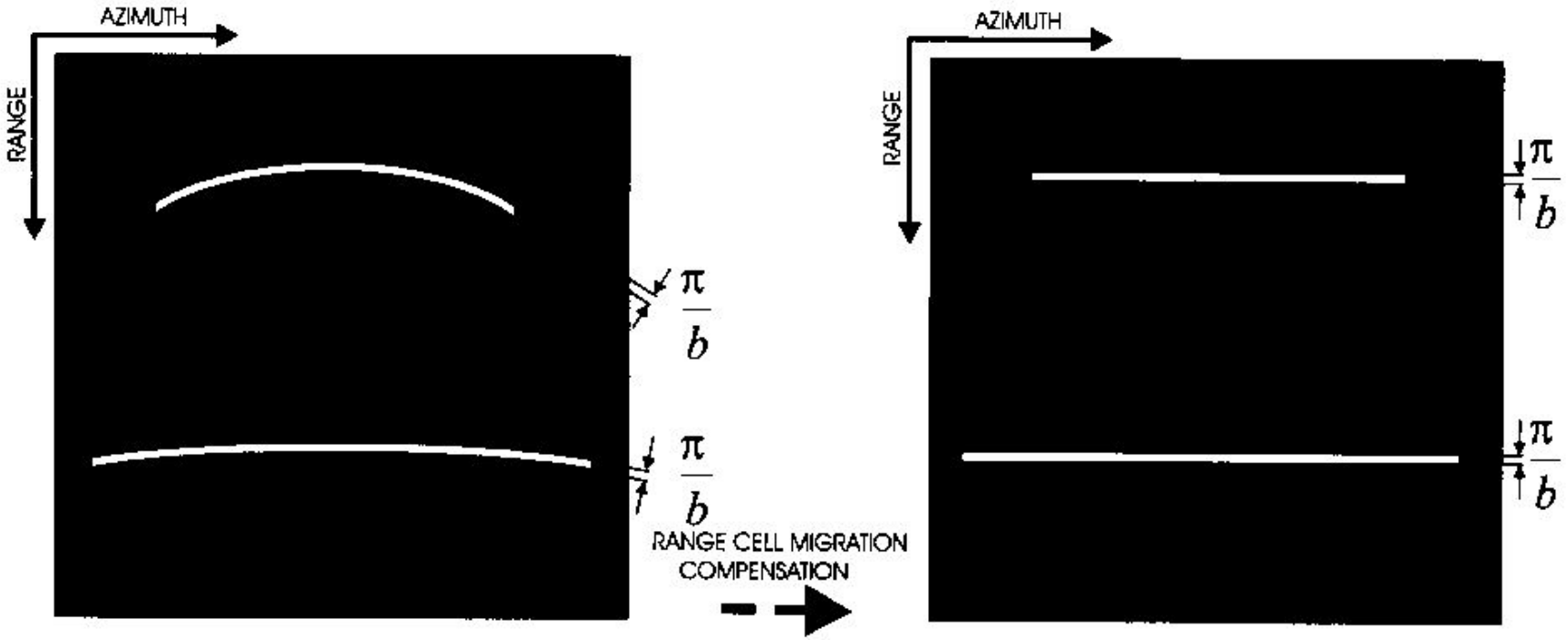

FIGURE 2A Two point targets, at different ranges, over an absorbing background. Range cell migration compensation.

Basic SAR image formation processes

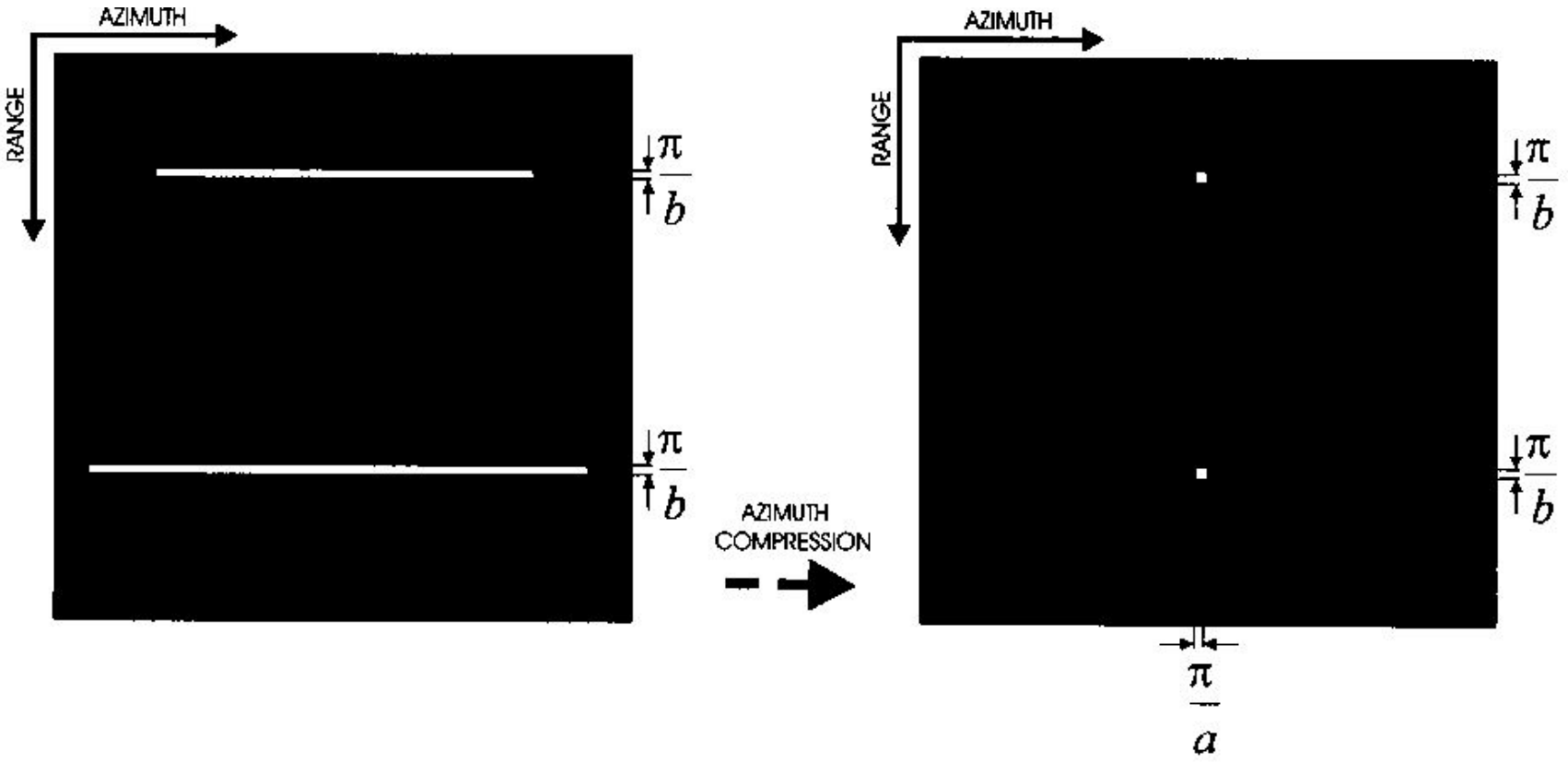

FIGURE 2B Same as Figure 2A. Azimuth compression.

Optical image-formation processing

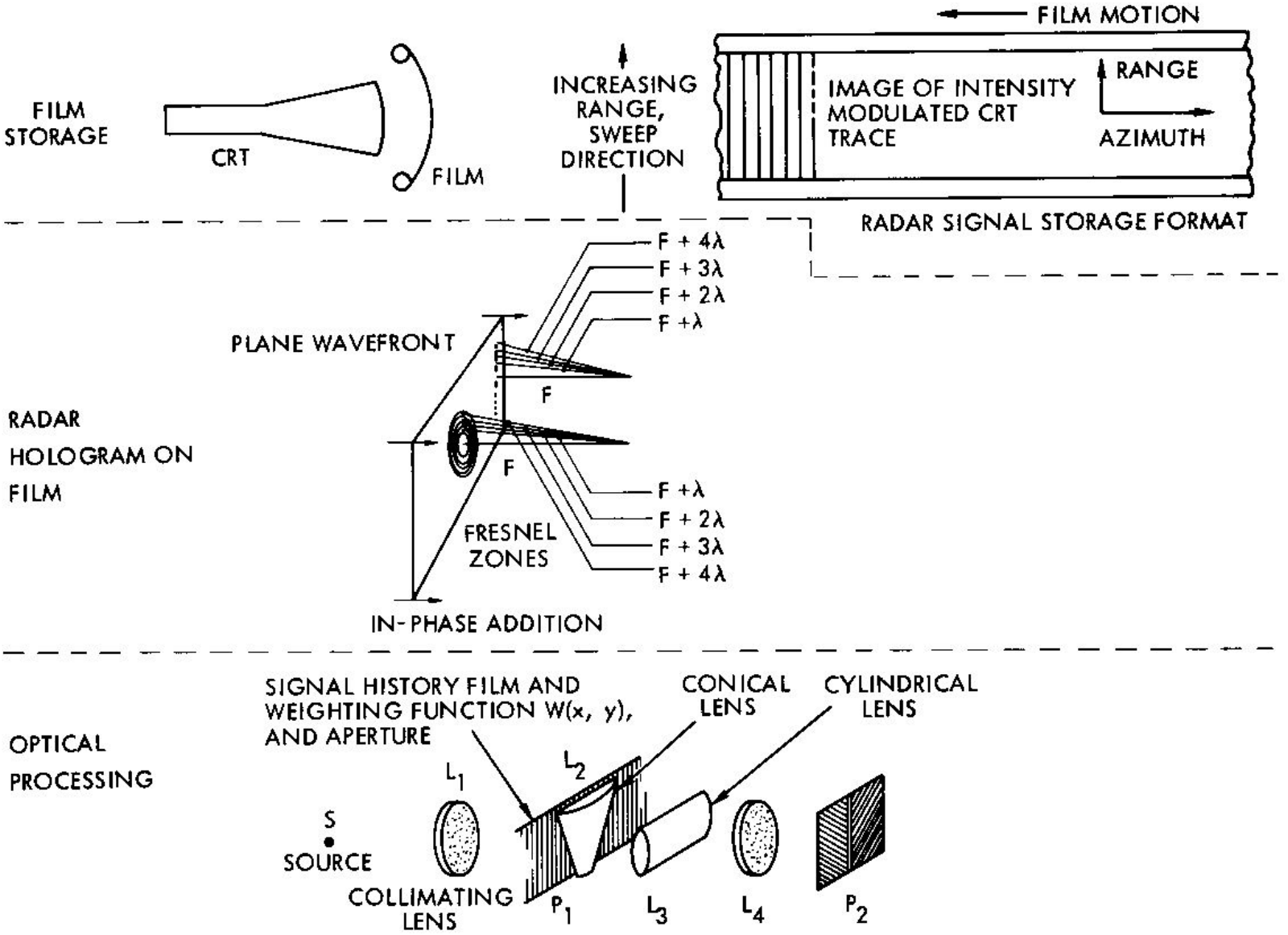

Figure 15 **Simultaneous Pulse Compression and Beam Sharpening (Optical Processing)**

Demodulated baseband SAR signal

[from *Digital processing of synthetic aperture radar data*, by Cumming and Wong, 2005]

Time domain representation

After removing the radar carrier $\cos(2\pi f_o \tau)$ from the received signal, the demodulated, complex, baseband signal from a single point target can be represented as

$$s_0(\tau,\eta) = A_0 \; w_r\Big(\tau - 2R(\eta)/c\Big) \; w_a(\eta-\eta_c) \times \exp\{-j\,4\pi\, f_0\, R(\eta)/c\} \; \exp\left\{j\pi\, K_r \left(\tau - 2R(\eta)/c\right)^2\right\} \quad (4.39)$$

where

- τ : range (fast) time, s
- η : azimuth (slow) time relative to the time of closest approach, s
- A_o: complex constant
- $w_r(\tau)$: envelope of the transmitted radar pulse
- $w_a(\eta)$: antenna's azimuth beam pattern
- $R(\eta)$: slant range in time domain, m
- η_c : beam center crossing time relative to the time of closest approach, s
- f_o: carrier frequency, Hz
- K_r : FM rate of transmitted pulse chirp, Hz/s

Demodulated baseband SAR signal

includes R^{-4} and target RCS factors

transmit waveform amplitude

antenna gain variation over synthetic aperture

$$s_0(\tau,\eta) = A_0\, w_r\Big(\tau - 2R(\eta)/c\Big)\; w_a(\eta-\eta_c)$$
$$\times\; \exp\{-j\,4\pi\, f_0\, R(\eta)/c\}\; \exp\left\{j\pi\, K_r\left(\tau - 2R(\eta)/c\right)^2\right\} \qquad (4.39)$$

range-dependent phase component

quadratic phase term due to transmitted chirp waveform

The instantaneous slant range is

$$R(\eta) = \sqrt{R_0^2 + V_r^2\,\eta^2} \approx R_0 + \frac{V_r^2\,\eta^2}{2\,R_0} \qquad (5.1)$$

where

V_r: effective radar velocity (a positive scalar), m/s

R_o: slant range at closest approach, m

SAR signal spectrum

[from *Digital processing of synthetic aperture radar data*, by Cumming and Wong, 2005]

Frequency-domain represention

For reasons of efficiency, many SAR processing algorithms operate in the frequency domain.

For the low-squint case, the two-dimensional frequency spectrum of the received SAR signal is

$$S_{2\mathrm{df}}(f_\tau, f_\eta) = W_r(f_\tau)\, W_a(f_\eta - f_{\eta_c}) \exp\{j\,\theta_{2\mathrm{df}}\} \tag{5.13}$$

where $\theta_{2\mathrm{df}}$, the phase function in the two-dimensional frequency domain, is

$$\theta_{2\mathrm{df}} \approx \frac{\pi f_\eta^2}{K_a'} - \frac{\pi f_\tau^2}{K_r} - \frac{4\pi (f_0 + f_\tau) R_0}{c} \tag{5.11}$$

and K_a', the azimuth FM rate in the frequency domain, is`

$$K_a' = \frac{2 V_r^2 (f_0 + f_\tau)}{c R_0} \tag{5.12}$$

SAR signal spectrum

Also

f_τ : range frequency, Hz, where $-F_r/2 \le f_\tau \le F_r/2$

F_r : range sampling frequency, Hz

f_η : azimuth (Doppler) frequency, Hz

$f_{\eta c}$: absolute Doppler centroid frequency, Hz

$W_r(f_\tau)$: envelope of the radar data's range spectrum

$W_a(f_\eta)$: envelope of the antenna's beam pattern Doppler spectrum

The relationship between azimuth time to frequency is

$$f_\eta \approx -K_a \eta \qquad (5.4)$$

where

$$K_a \approx \frac{2V_r^2}{\lambda R_0} = \frac{2V_r^2 f_0}{c R_0} \qquad (5.3)$$

SAR signal spectrum

envelope of the radar data's range spectrum

antenna's beam pattern envelope in Doppler spectrum

$$S_{2df}(f_\tau, f_\eta) = W_r(f_\tau)\, W_a(f_\eta - f_{\eta_c})\, \exp\{j\,\theta_{2df}\} \qquad (5.13)$$

phase function in two-dimensional frequency domain

$$\theta_{2df} \approx \frac{\pi f_\eta^2}{K_a'} - \frac{\pi f_\tau^2}{K_r} - \frac{4\pi (f_0 + f_\tau) R_0}{c} \qquad (5.11)$$

quadratic phase term due to azimuth chirp

quadratic phase term due to transmitted chirp

range-dependent phase component

Matched filter processing

Given an understanding of the characteristics of the ideal SAR signal, an ideal matched-filter can be applied using correlation to produce a bandwidth limited impulse response.

However this process has limitations as the characteristics of the ideal matched-filter varies with the target's position in range and azimuth.

So while such correlation processing is theoretically possible, it is not computationally efficient and is not appropriate when large-scale image-formation processing is required, e.g., from a spaceborne SAR system.

Range Doppler domain spectrum

[from *Digital processing of synthetic aperture radar data*, by Cumming and Wong, 2005]

Range Doppler-domain representation

The range-Doppler domain is useful for range-Doppler image formation algorithms.

The range-Doppler domain signal is

$$S_{\mathrm{rd}}(\tau, f_\eta) \approx w_r\left(\tau - \frac{2\,R_{\mathrm{rd}}(f_\eta)}{c}\right) W_a(f_\eta - f_{\eta_c}) \exp\{j\,\theta_{\mathrm{rd}}\} \qquad (5.9)$$

where θ_{rd}, the azimuth phase function in the range-Doppler domain, is

$$\theta_{\mathrm{rd}} \approx \frac{\pi\,f_\eta^2}{K_a} + \pi\,K_r\left[\tau - \frac{2\,R_{\mathrm{rd}}(f_\eta)}{c}\right]^2 - \frac{4\pi\,R_0}{\lambda} \qquad (5.8)$$

and $R_{\mathrm{rd}}(f_\eta)$, the slant range in the range-Doppler domain, represents the range cell migration in this domain

$$R_{\mathrm{rd}}(f_\eta) \approx R_0 + \frac{\lambda^2\,R_0}{8\,V_r^2}\,f_\eta^2 \qquad (5.10)$$

Range migration

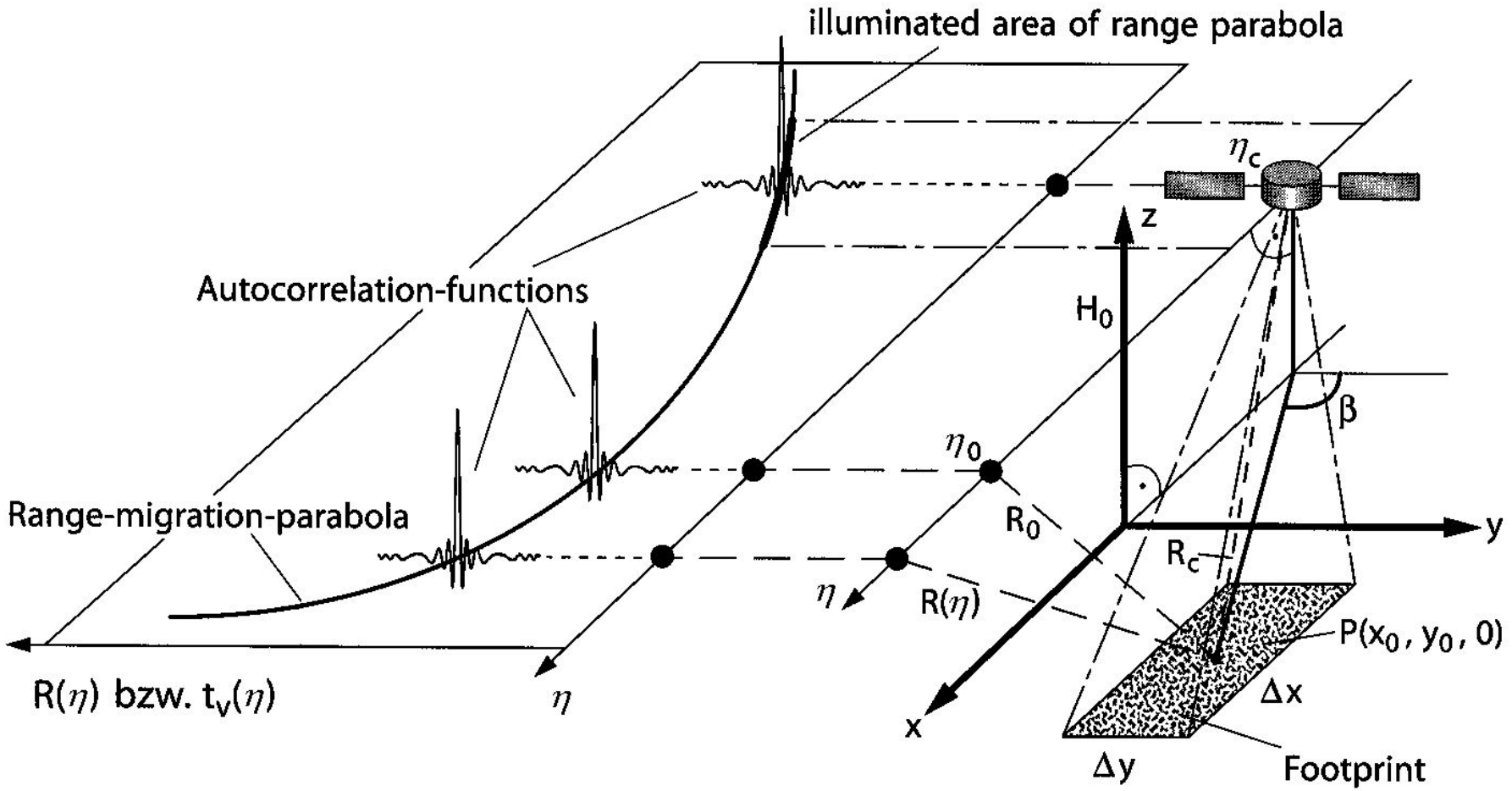

Image 3.11: Illustration of the range migration

Range-dependent range migration

B_{az} : azimuth bandwidth
B_r : transmitted pulse bandwidth
η_o : azimuth time when target perpendicular
η_c : azimuth time when target in epicenter of azimuth signal
$t_v(\eta)$: time delay between Tx and Rx signal, = $2R(\eta)/c$
$R(\eta_o)$: azimuth time-dependent distance

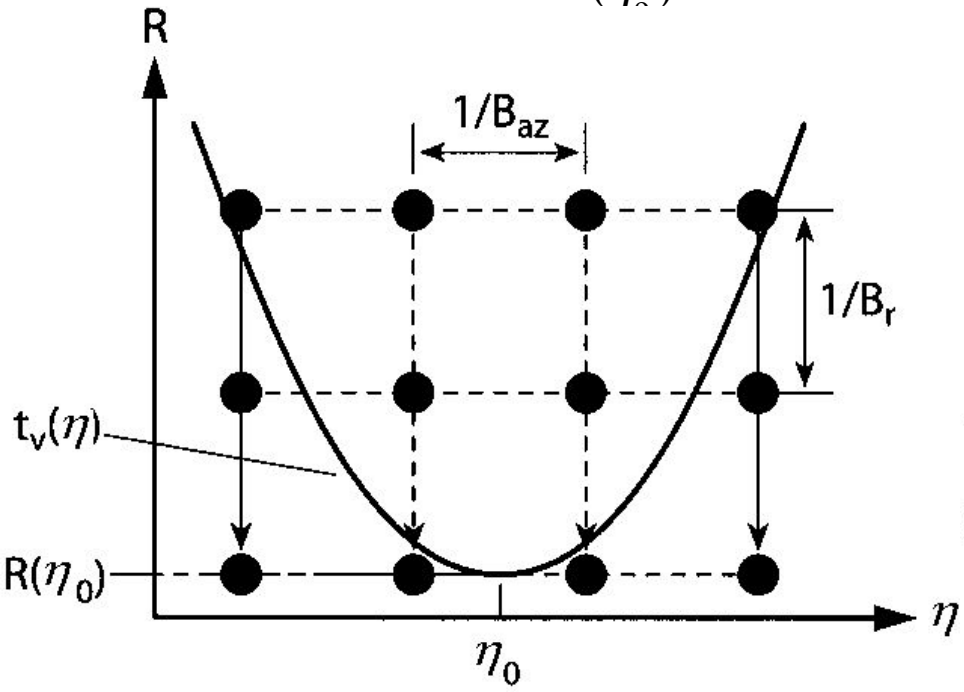

Image 3.12: Near-range parabola

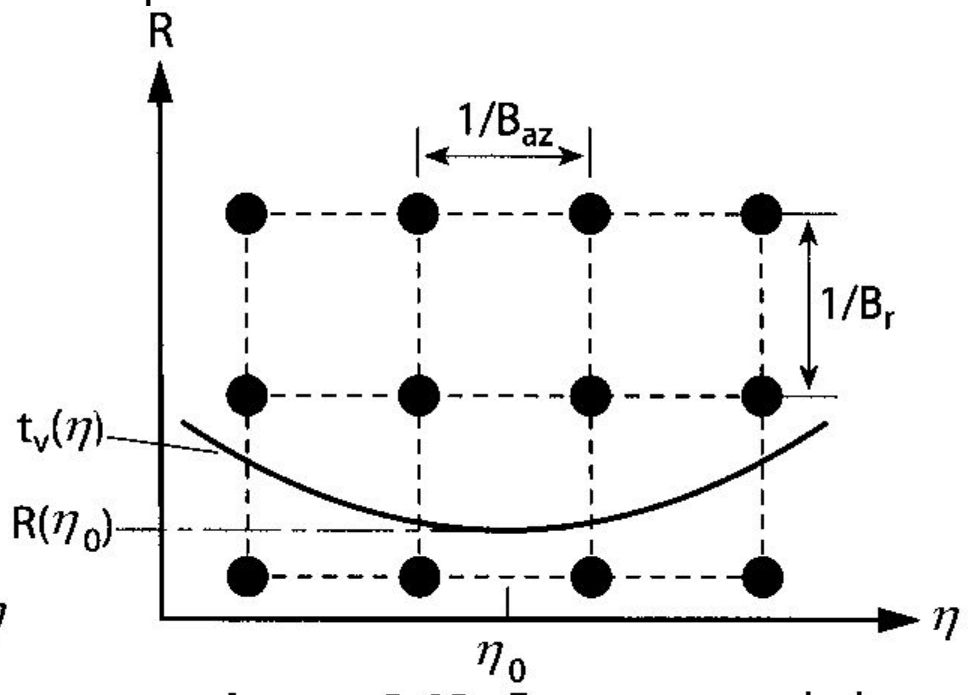

Image 3.13: Far-range parabola

Range-Doppler processing

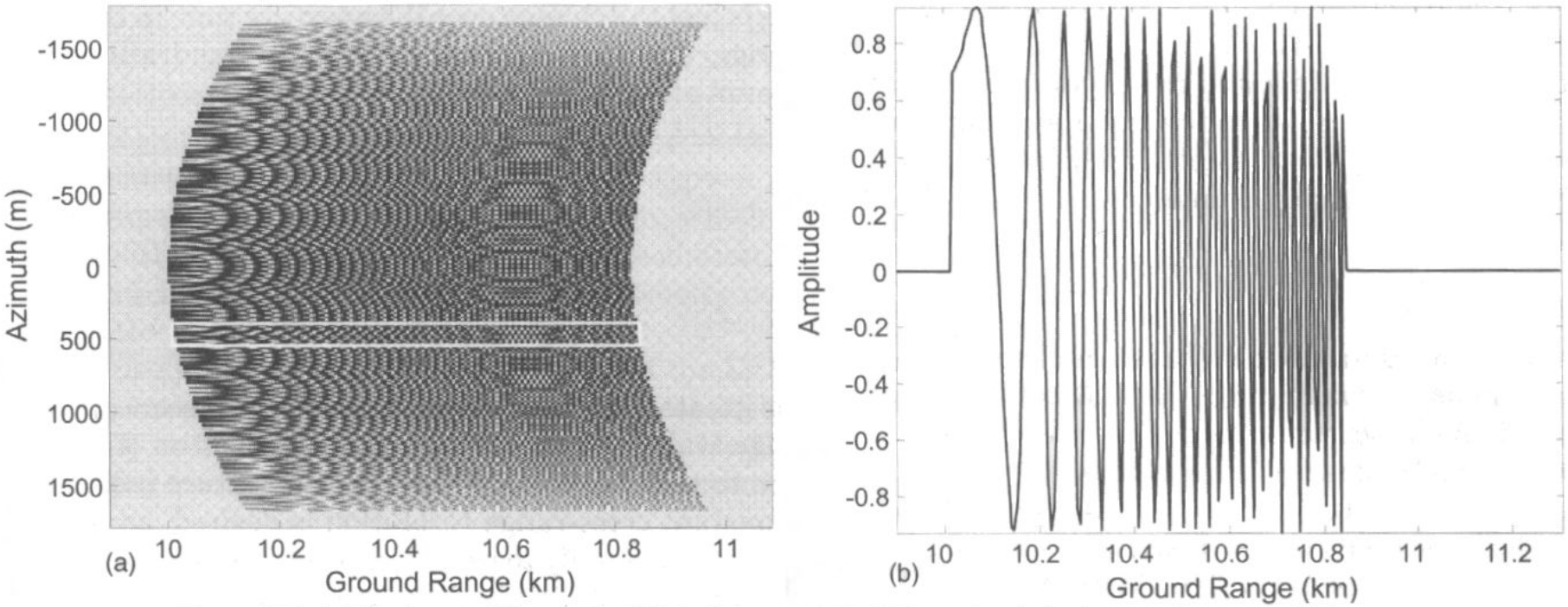

Figure 8.16 (*a*) Real part of the received data from a point scatterer located at $x_P = 0$, $y_{gP} = 10$ km. (*b*) Fast-time slice at azimuth position $u = 500$ m. (See text for radar parameters.)

Range-Doppler processing

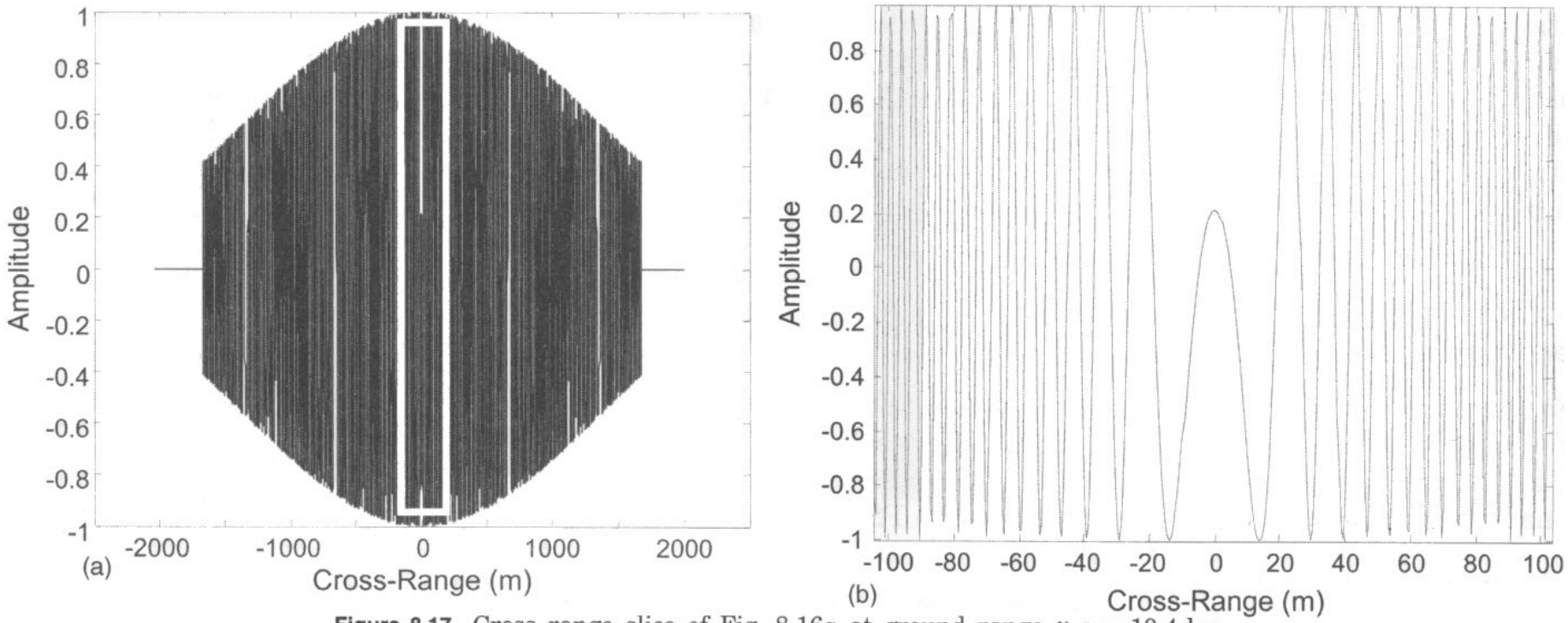

Figure 8.17 Cross range slice of Fig. 8.16*a* at ground range $y_{gP} = 10.4$ km. (*a*) Complete slice. (*b*) Central portion of the slice.

Range-Doppler processing

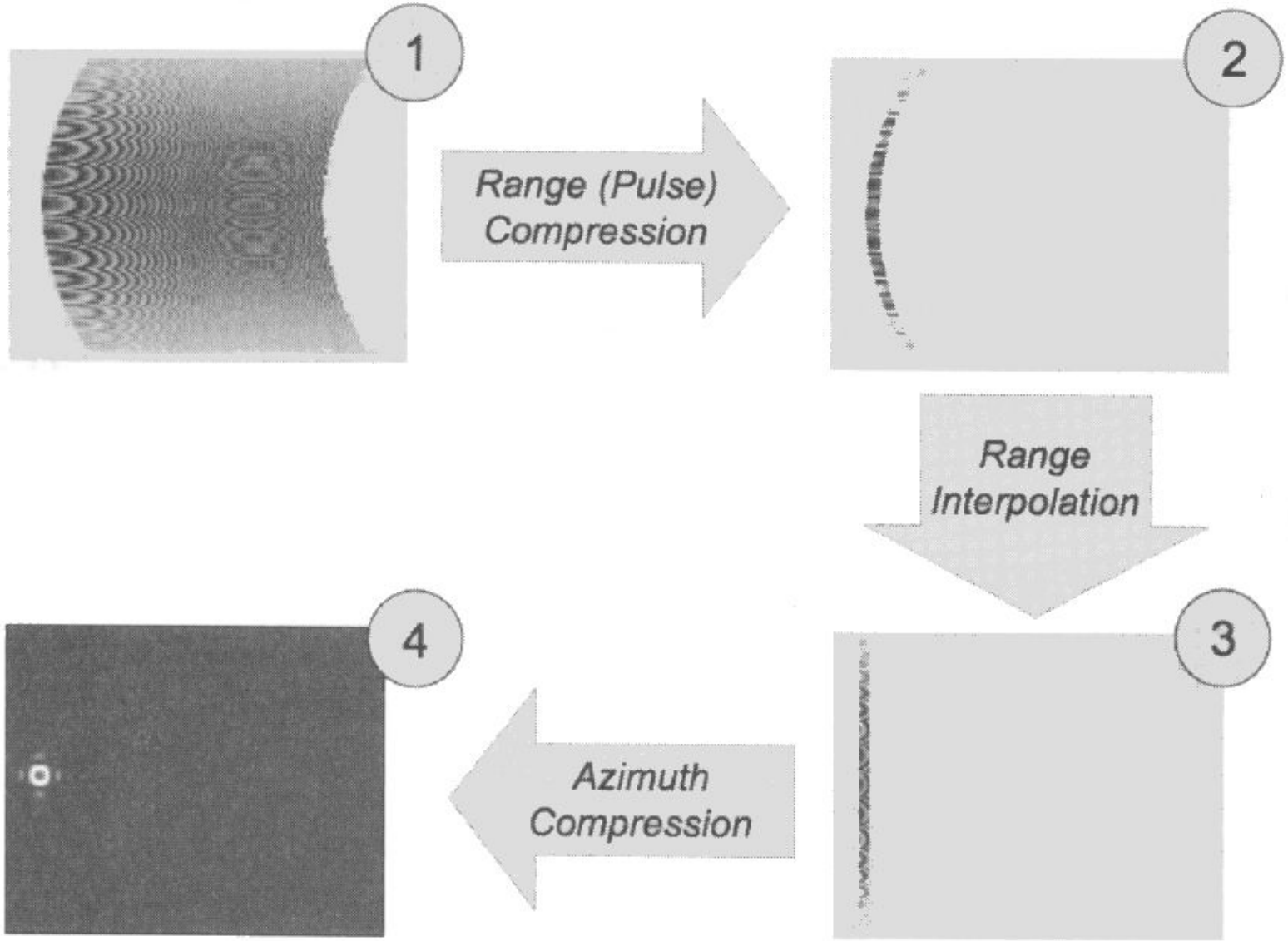

Figure 8.28 Notional illustration of sequence of operations in classic range-Doppler algorithm.

Range-Doppler algorithm

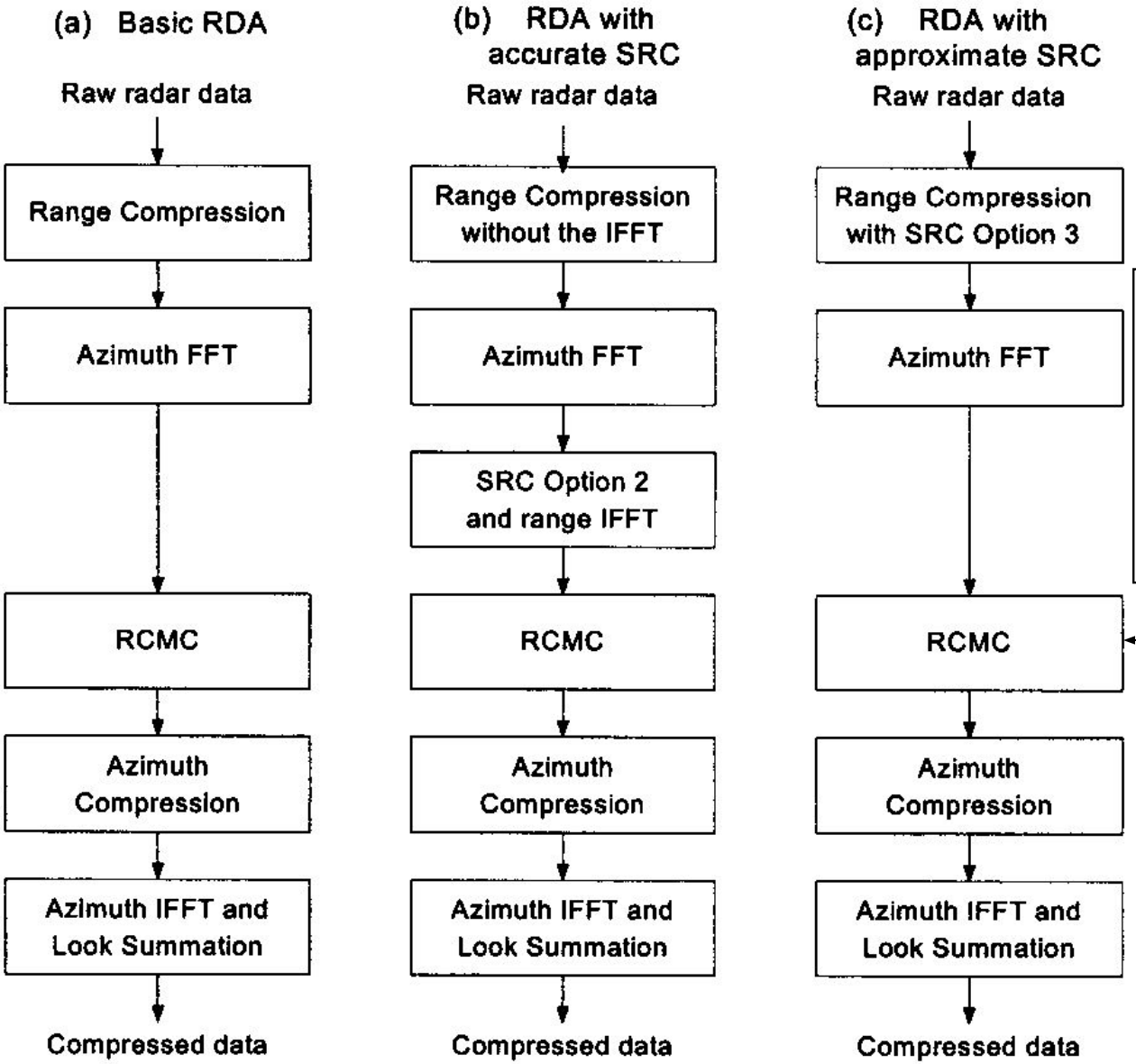

Figure 6.1: Functional block diagram of the RDA, showing three implementations.

RCMC: range cell migration compensation SRC: secondary range compression

Range-cell migration compensation

Part of the migration compensation requires a re-sampling of the range-compressed pulse using an interpolation process.

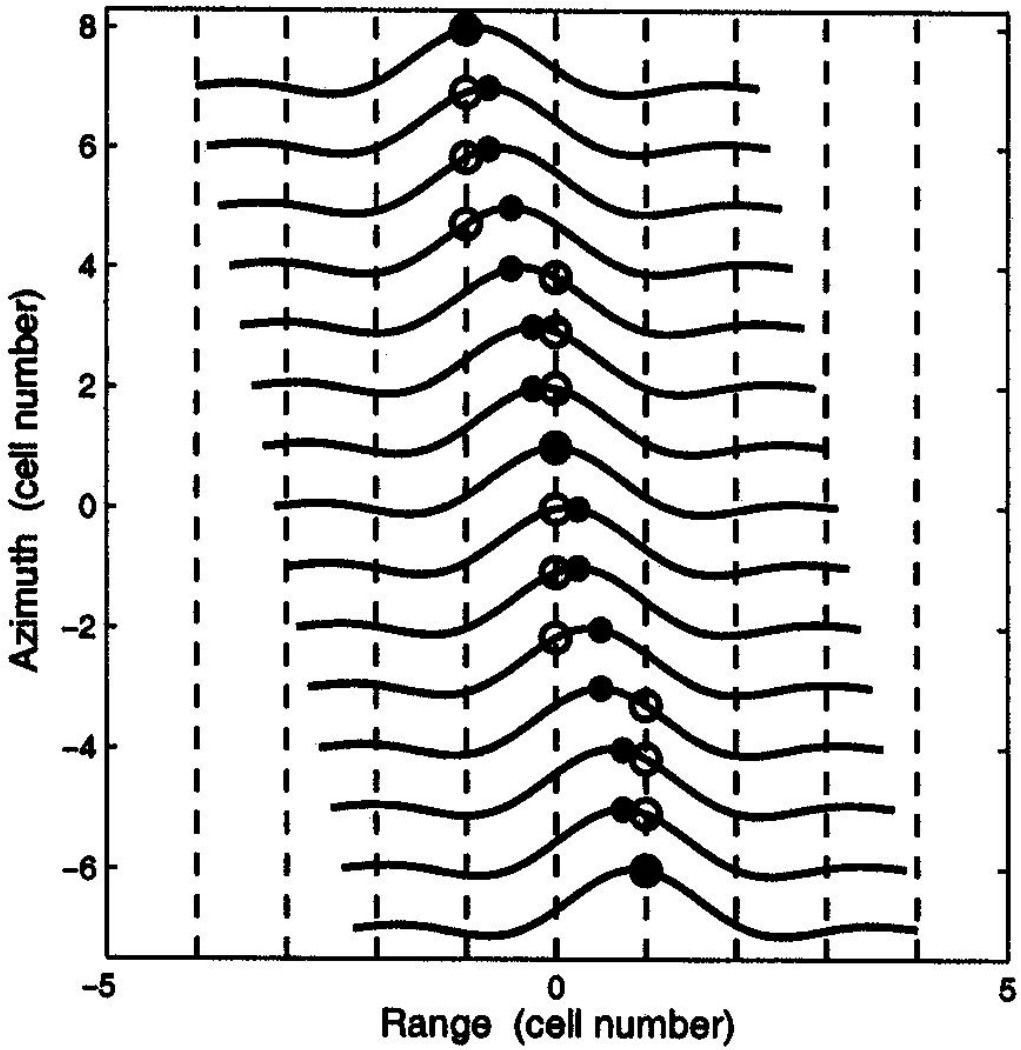

Figure 6.7: Sampling of a range-compressed pulse as it migrates through range cells.

Chirp scaling algorithm

The range-Doppler algorithm was the first digital algorithm developed for civilian satellite SAR processing and is still the most widely used.

However disadvantages (high computational load, limited accuracy secondary-range compression in high-squint and wide-aperture cases) prompted the development of the chirp-scaling algorithm to eliminate interpolation from the range-cell migration compensation step.

As the name implies it uses a scaling principle whereby a frequency modulation is applied to a chirp-encoded signal to achieve a shift or scaling of the signal.

Chirp scaling algorithm

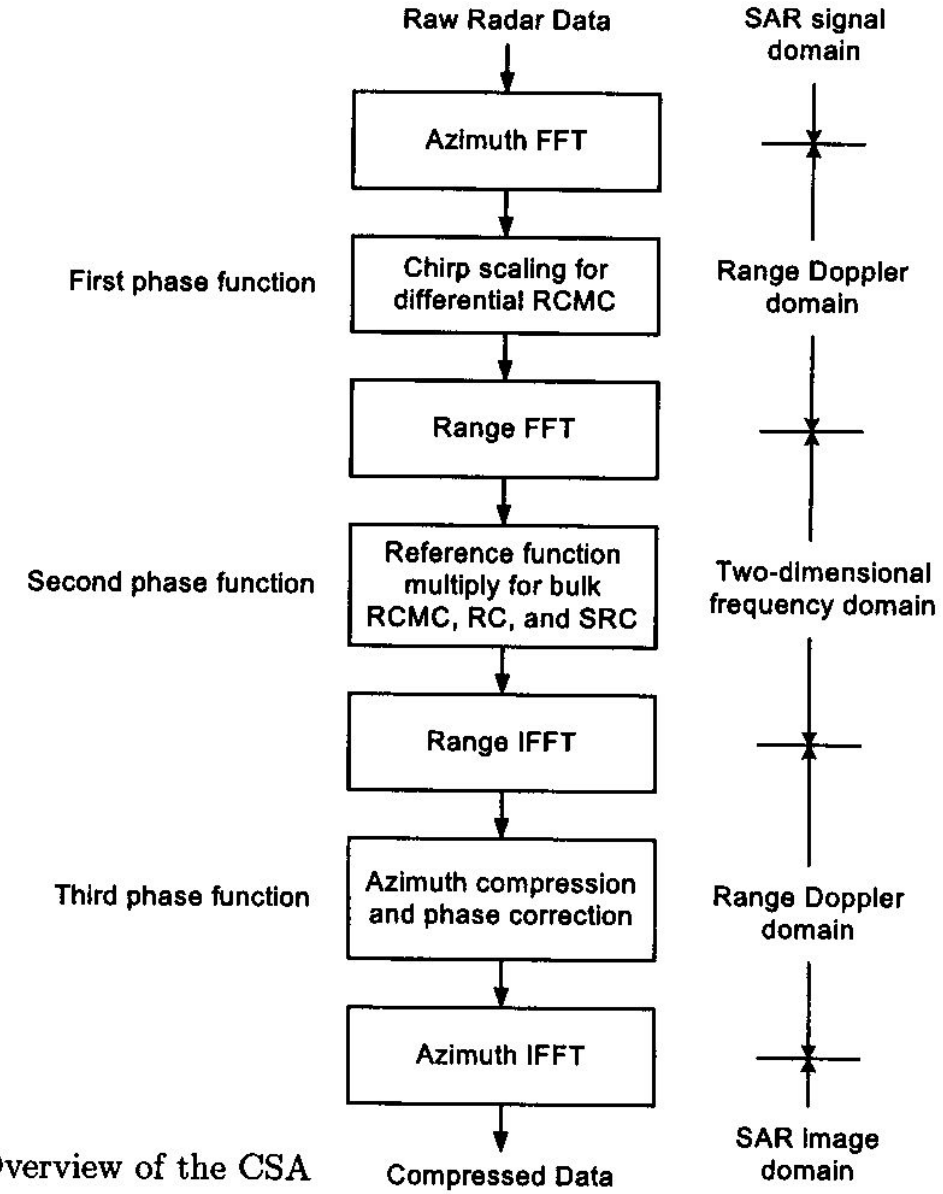

Figure 7.1: Overview of the CSA

Chirp scaling algorithm

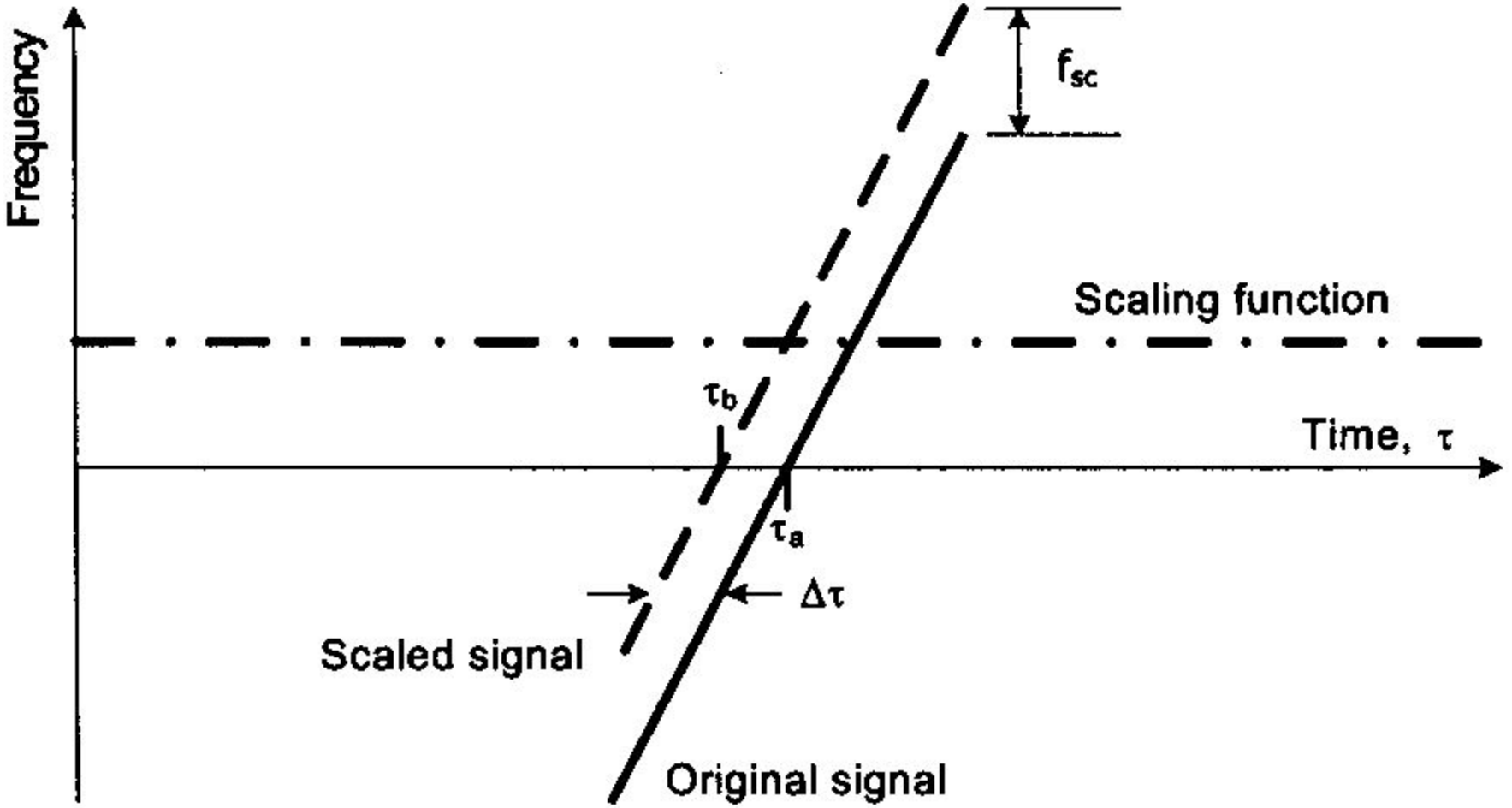

Figure 7.2: Shifting effect of a constant-frequency scaling function.

Chirp scaling algorithm

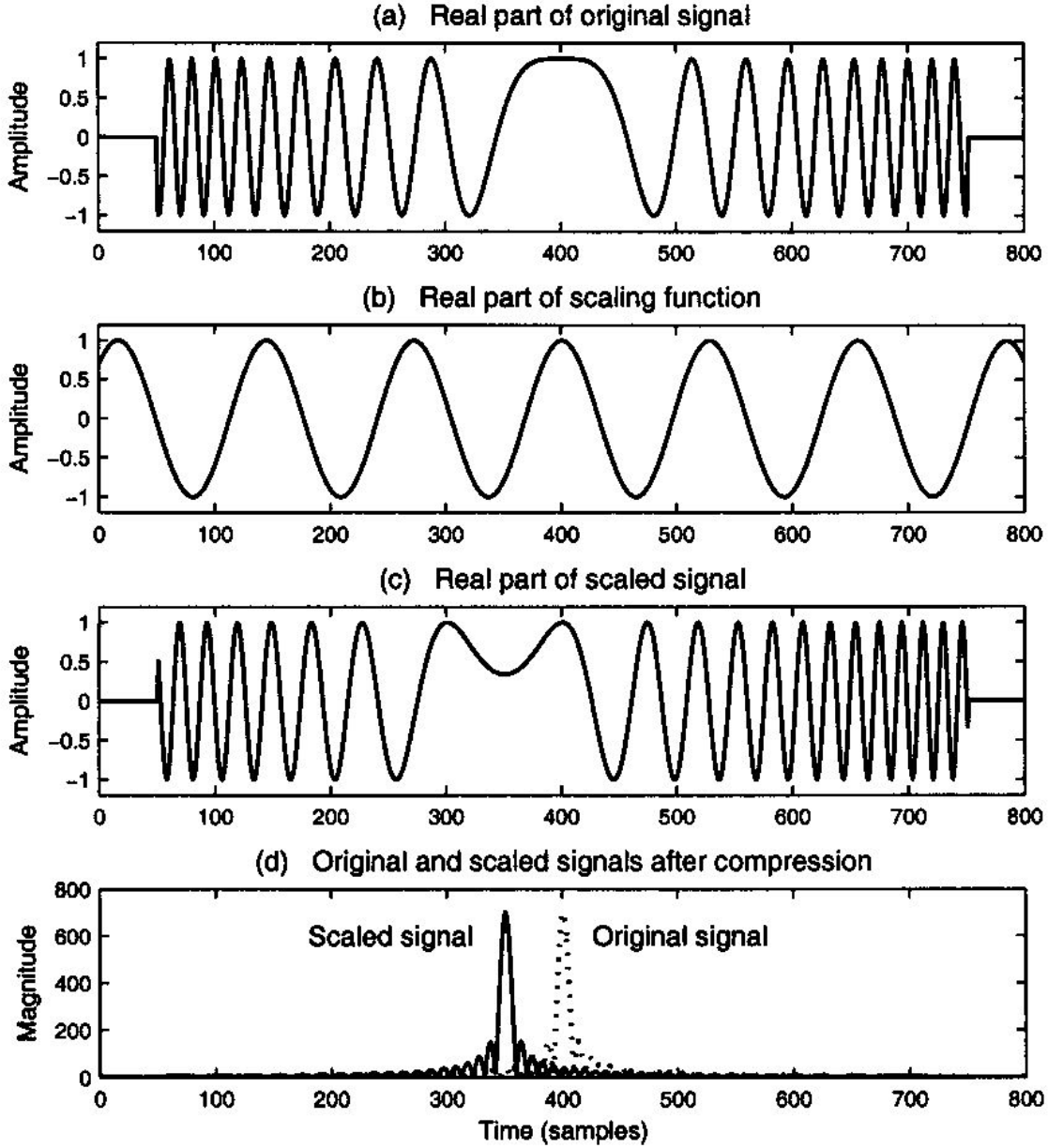

Figure 7.3: A simple example of target shift after scaling and compression.

Chirp scaling algorithm

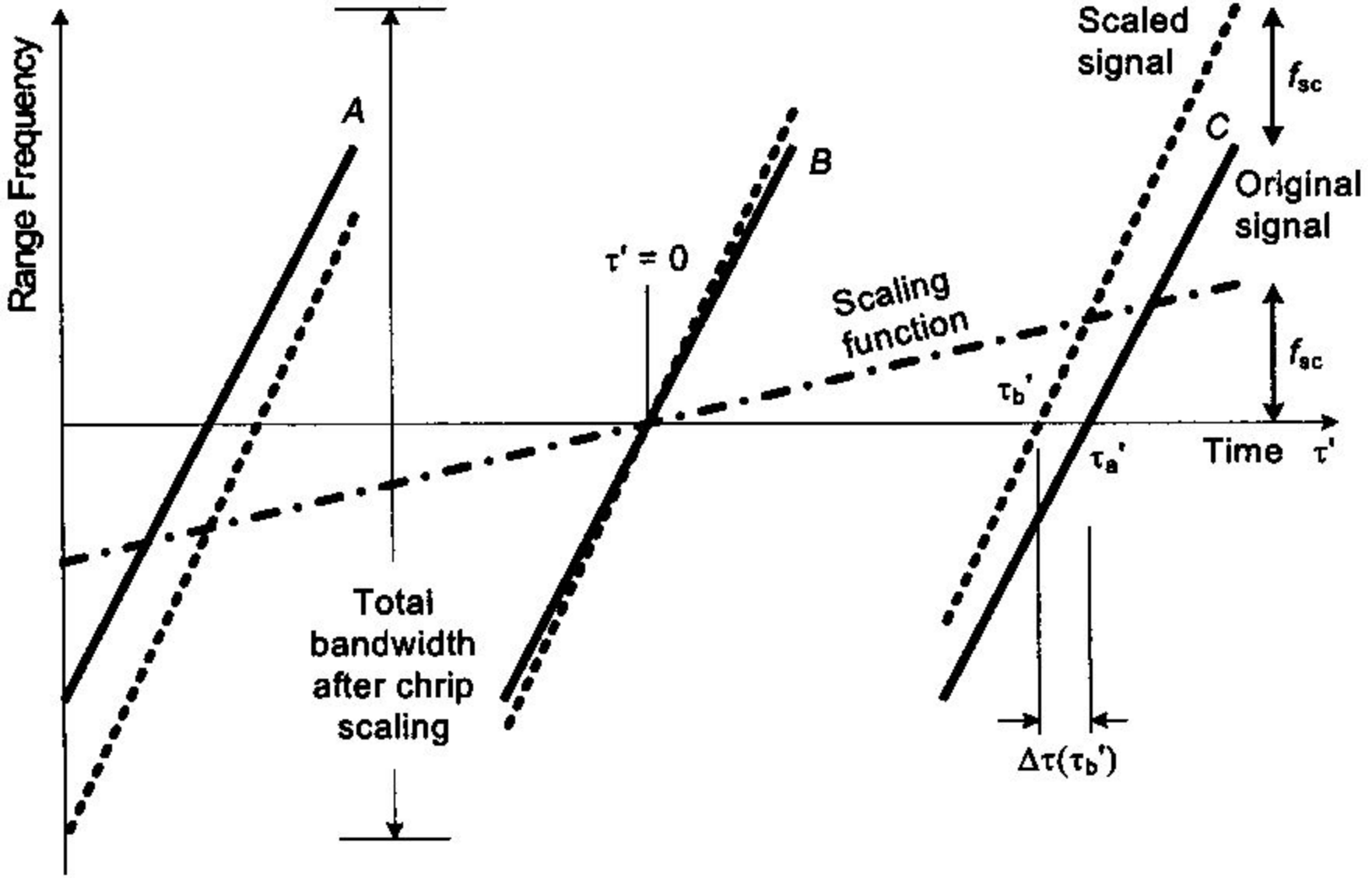

Figure 7.4: Action of a linear FM scaling function.

Chirp scaling algorithm

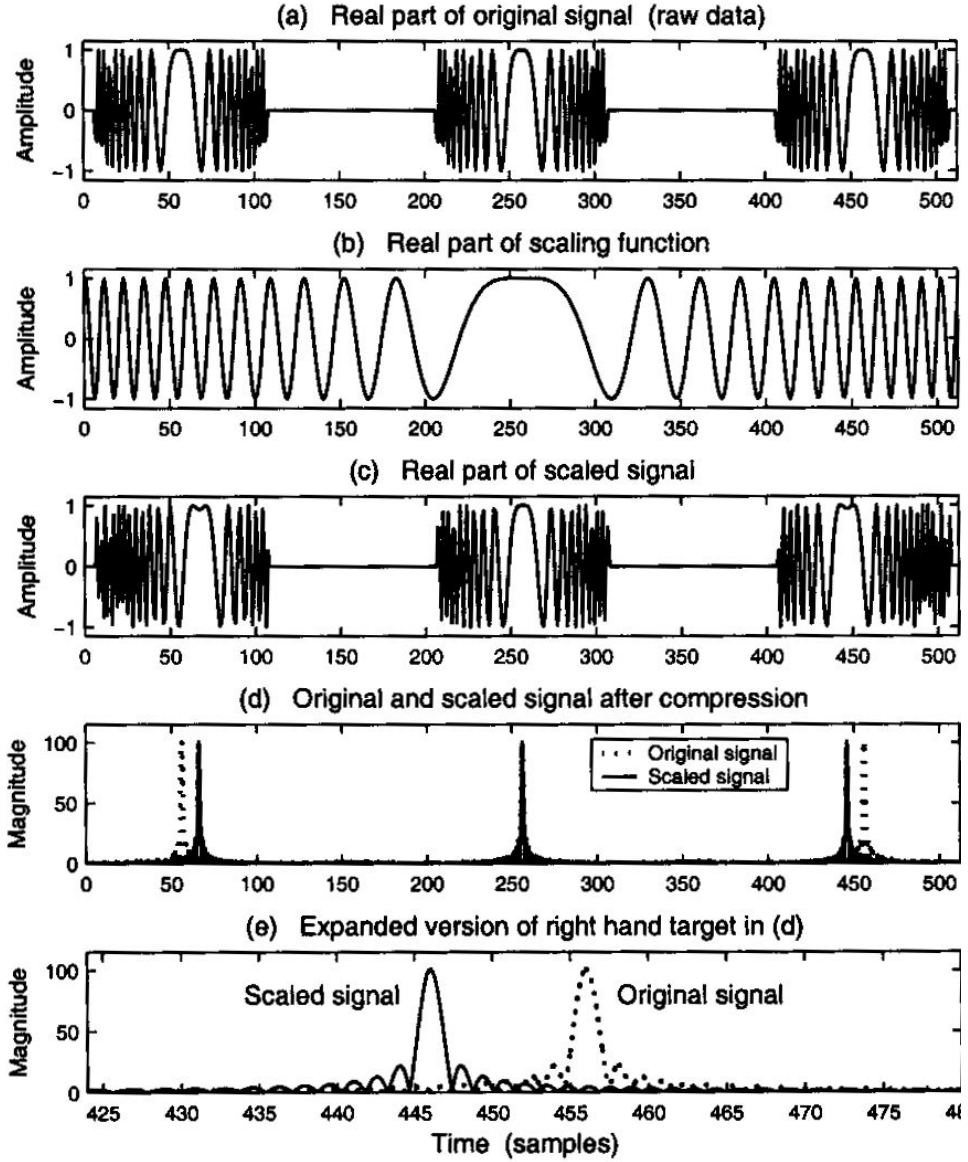

Figure 7.5: Shifting of targets by a linear FM scaling function.

Range-cell migration compensation

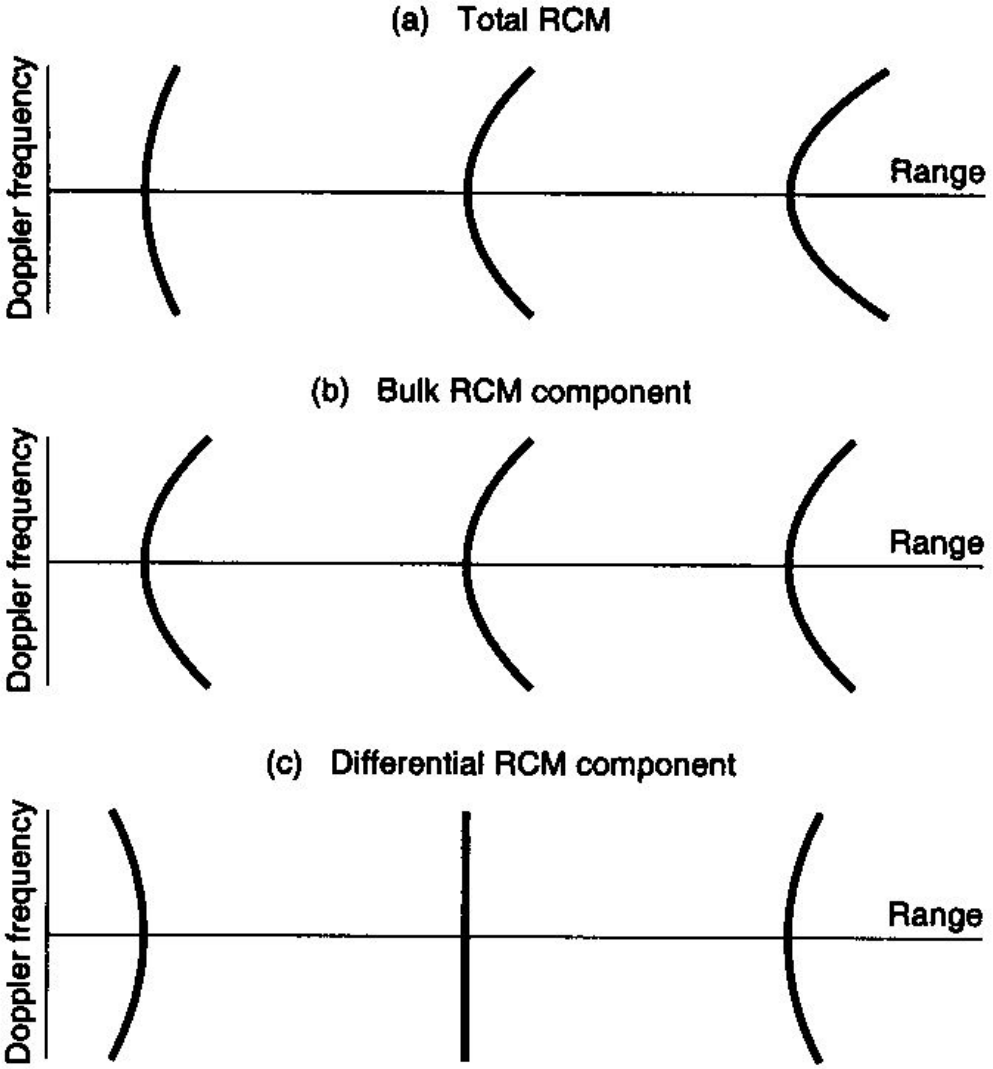

Figure 7.6: The total RCM expressed as the sum of a range-invariant bulk RCM and a range-variant differential RCM.

Omega-K algorithm (WKA)

The chirp-scaling algorithm assumes a specific form of the SAR signal in the range Doppler domain, which involves approximations that may become invalid for wide apertures or high squint angles.

The Omega-K algorithm uses a special operation in the two-dimensional frequency domain to correct range dependent range-azimuth coupling and azimuth frequency dependence.

The WKA uses a focusing step wherein a reference function is multiplied to provide focusing of a selected range. Targets at the reference range are correctly focused while targets at other ranges are partially focused.

Stolt interpolation is used to focus the remainder of the targets.

Omega-K algorithm (WKA)

Illustration of the range/azimuth cross coupling using the raw phase history from a point target.
Range-cell migration introduces a phase change into the azimuth samples in addition to the normal phase encoding.
The RCM cross coupling creates an additional azimuth phase term which affects the azimuth FM rate.

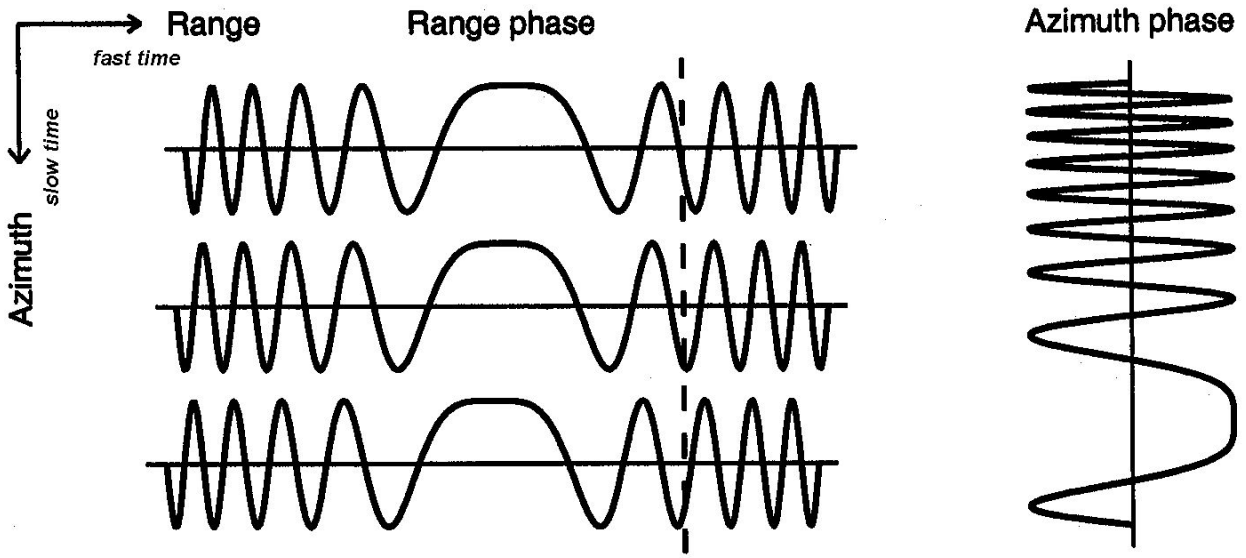

Figure 5.1: Phase coupling between range and azimuth.

From chirp pulse compression example

$$s(t) = \frac{a^2}{2} \cos\left(2\pi\left(f_c T + k\,T\,t - 0.5\,k\,T^2\right)\right)$$

Range-dependent phase terms

Omega-K algorithm (WKA)

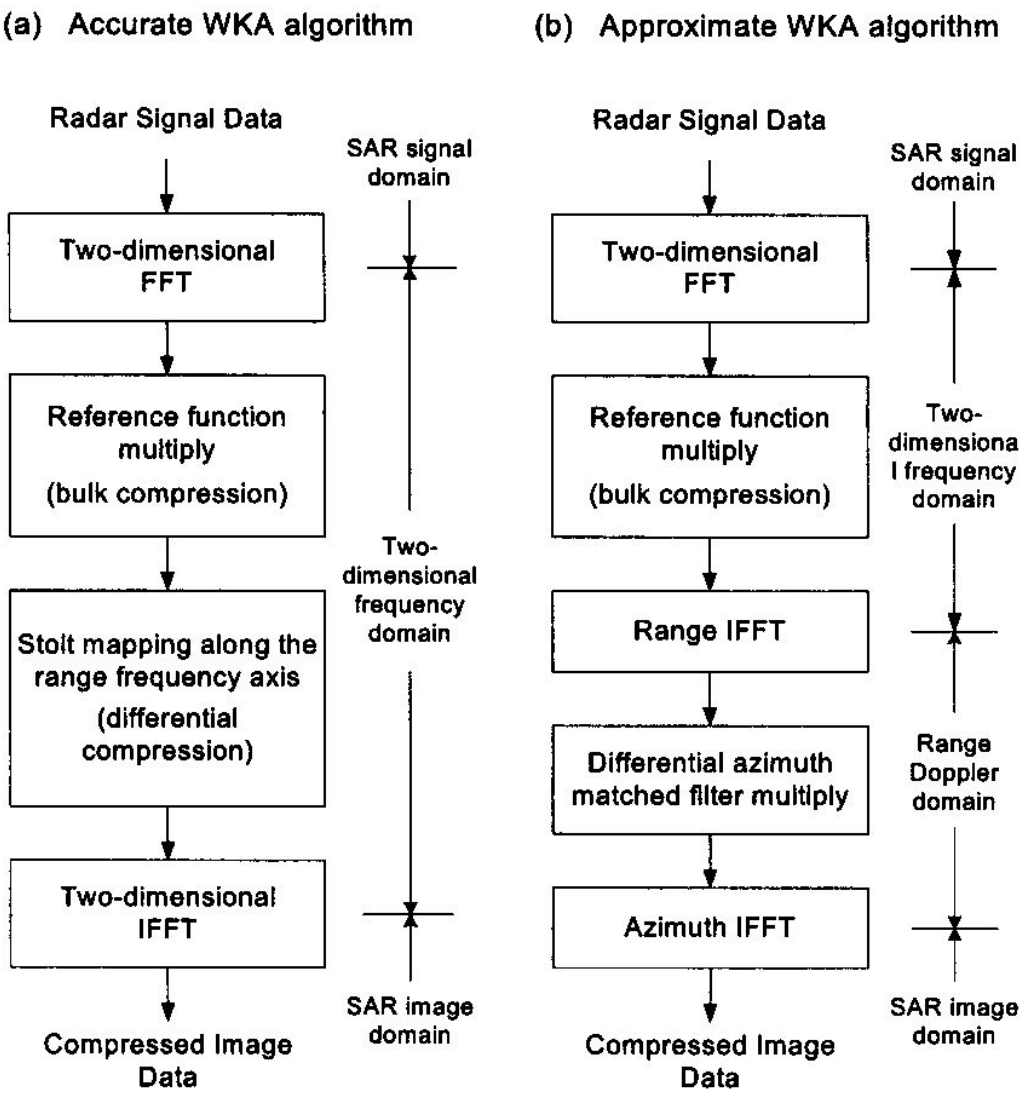

Figure 8.1: The major operations in the (a) accurate and (b) approximate forms of the omega-K algorithm.

Stolt interpolation

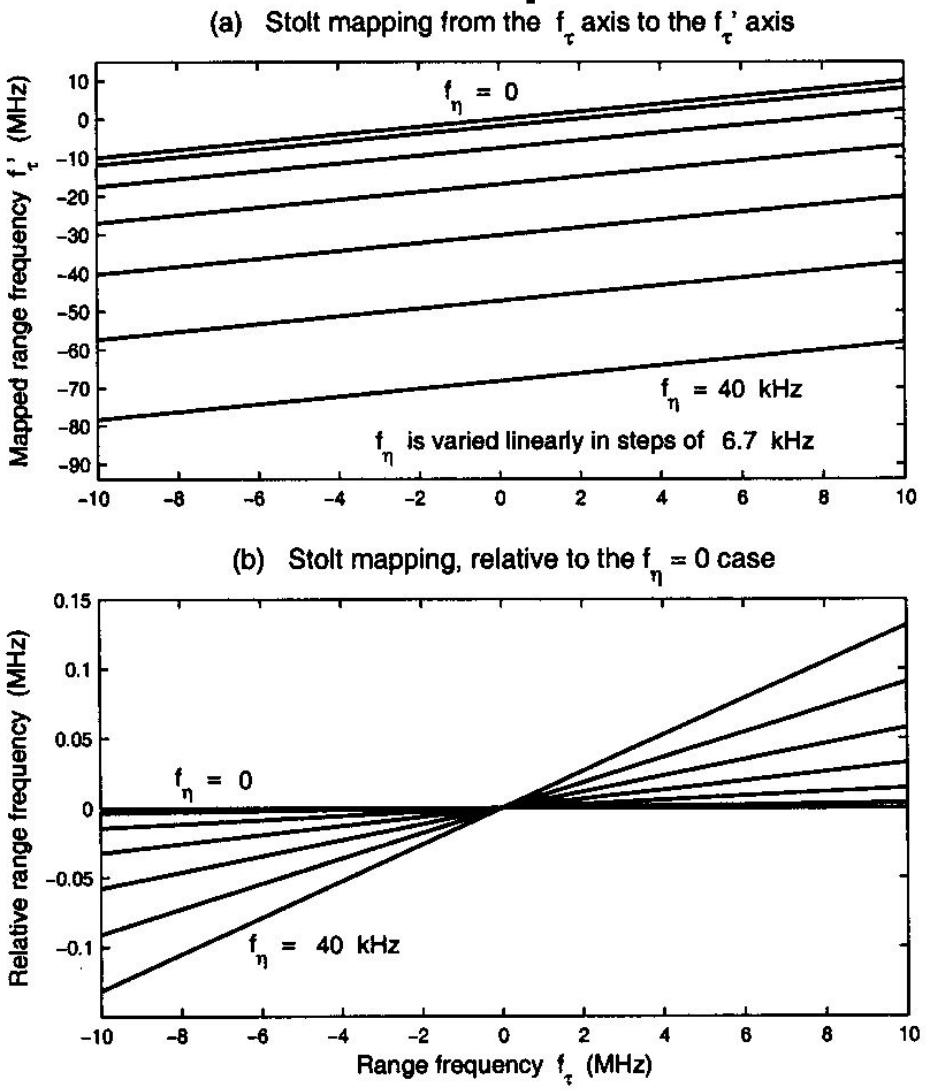

Figure 8.2: Illustrating the Stolt mapping of the variable f_τ onto the variable f'_τ of (8.5). Panel (b) shows the data of the upper plot with an expanded vertical scale, with the $f_\eta = 0$ curve subtracted and the offset at $f_\tau = 0$ of each curve subtracted as well.

Stolt interpolation

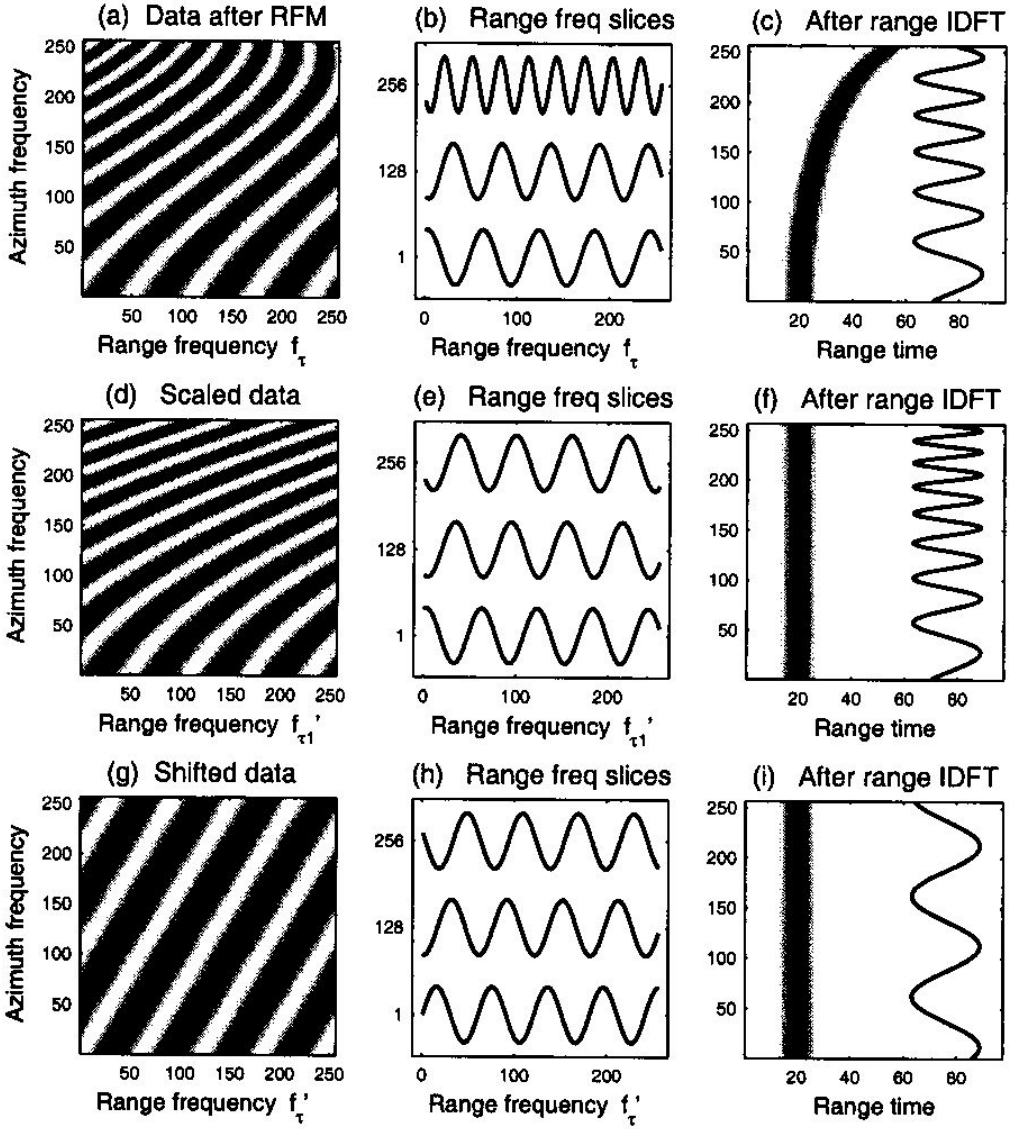

Figure 8.5: Illustration of the scaling and shifting effect of the Stolt interpolation.

Stolt interpolation

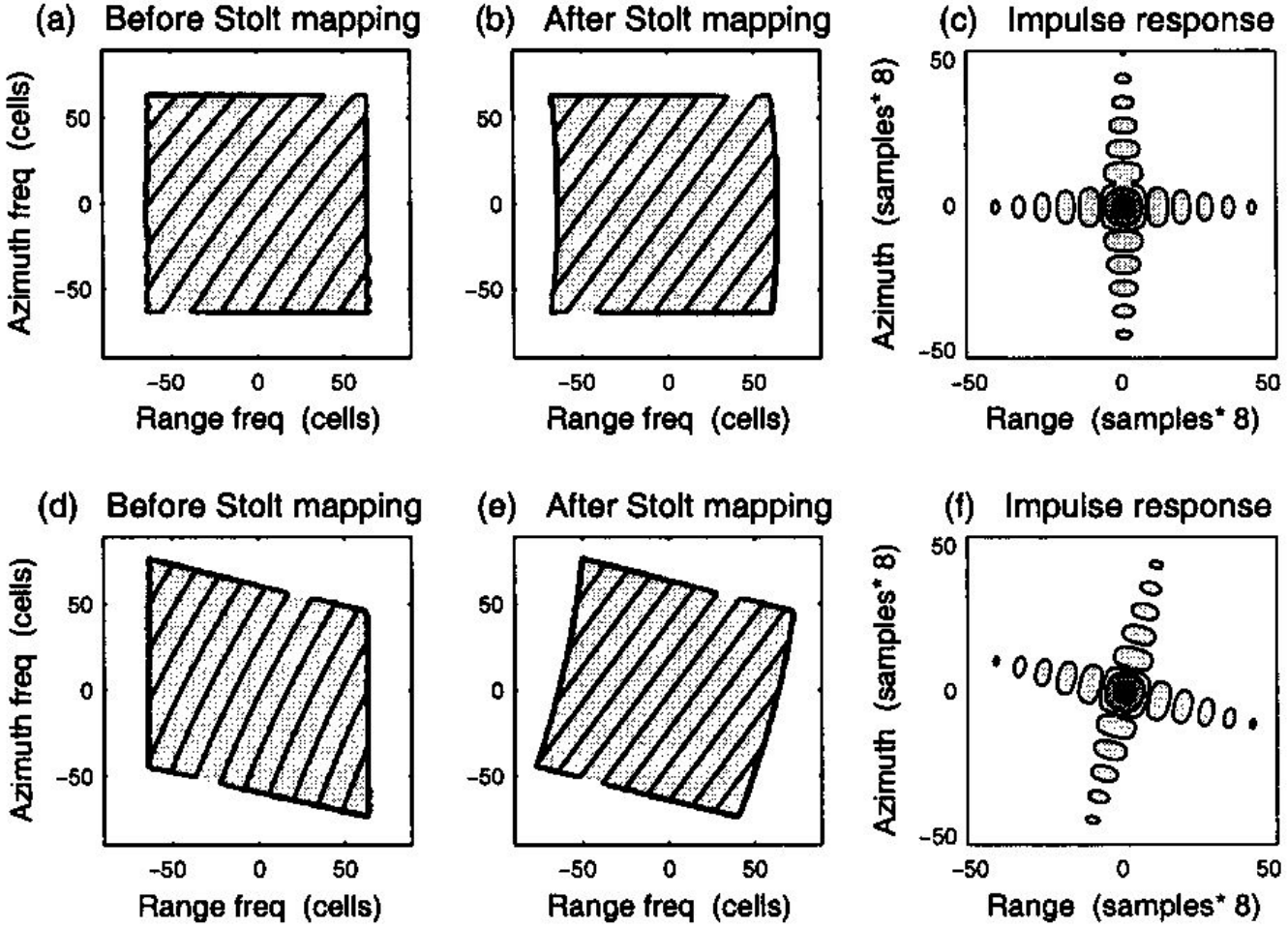

Figure 8.6: Two-dimensional spectra of a target and the impulse response after compression. The top row (a–c) is the zero squint case, while the bottom row (d–f) illustrates the skew of the spectrum when significant squint is present. The solid lines in the two leftmost columns represent phase contours.

Comparison of IFP algorithms

Table 11.1: Comparison of Processing Functions

	RDA appr. SRC	RDA accr. SRC	CSA	ωKA approx.	ωKA accurate
Solution form:	Hyperb. or P.S.	Hyperb. or P.S.	Hyperb. or P.S.	Hyperb.	Hyperb.
Azim MF					
- param.	R_0 var. V_r var.	R_0 var. V_r var.	R_0 var. V_r var.	R_0 var. V_r var.	R_0 var. V_r invar.(1)
- bulk	Phase $\times$ in (τ, f_η)	Phase $\times$ in (τ, f_η)	Phase $\times$ in (f_τ, f_η)	Phase $\times$ in (f_τ, f_η)	Phase $\times$ in (f_τ, f_η)
- residual	None	None	Phase $\times$ in (τ, f_η)	Phase $\times$ in (τ, f_η)	Interp. in (f_τ, f_η)
RCMC					
- param.	R_0 var. V_r var.	R_0 var. V_r var.	R_0 var. V_r invar.(2)	R_0 invar. V_r invar.	R_0 var. V_r invar.
- bulk	Interp. in (τ, f_η)	Interp. in (τ, f_η)	Phase $\times$ in (f_τ, f_η)	Phase $\times$ in (f_τ, f_η)	Phase $\times$ in (f_τ, f_η)
- residual	None	None	CS phase $\times$ in (τ, f_η)	Ignored	Interp. in (f_τ, f_η)
SRC					
- param.	R_0 invar. V_r invar. f_η invar.	R_0 invar. V_r invar. f_η var.	R_0 invar. V_r invar. f_η var.	R_0 invar. V_r invar. f_η var.	R_0 var. V_r invar. f_η var.
- bulk	Combine with rg MF	Phase $\times$ in (f_τ, f_η)	Phase $\times$ in (f_τ, f_η)	Phase $\times$ in (f_τ, f_η)	Phase $\times$ in (f_τ, f_η)
- residual	Ignored	Ignored	Ignored	Ignored	Interp. in (f_τ, f_η)

Hyperb: hyperbolic
P.S.: power series, i.e., parabolic

RCMC: range cell migration correction

SRC: secondary range compression

Notes: The range invariances in both cases (1) and (2) can be compensated. In case (1), a residual azimuth compression can be performed by a phase multiply. In case (2), a nonlinear perturbation function can be used.
P.S. means "Power Series."

Motion compensation

Imperfect trajectories during SAR data collection will distort the data set resulting in degraded images unless these imperfections are removed.

Removal of the effects of these imperfections is called motion compensation.

Motion compensation requires precise knowledge of the antenna's phase center over the entire aperture.

- For example vertical velocity will introduce an additional Doppler shift into the data that, if uncompensated, will corrupt along-track processing.
- Similarly a variable ground speed will result in non-periodic along-track sampling that, if uncompensated, will also corrupt along-track processing.

Knowledge of the antenna's attitude (roll, pitch, yaw angles) is also important as these factors may affect the illumination pattern as well as the position of the antenna's phase center.

Motion compensation

To provide position and attitude knowledge various instruments are used

- Gyroscopes (mechanical or ring-laser)
- Inertial navigation system (INS)
- Accelerometers
- GPS receiver

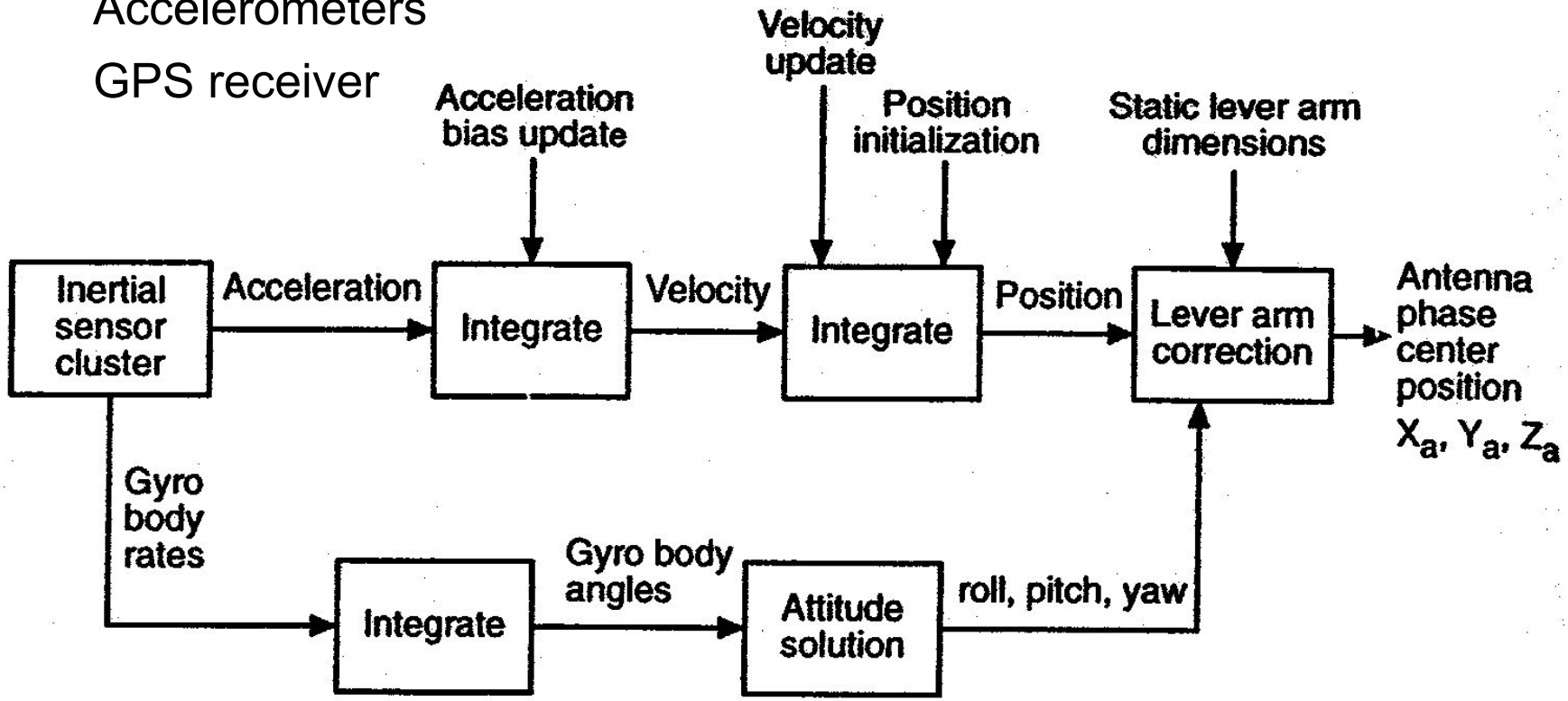

Figure 2.20 Motion computation procedure.

Motion compensation

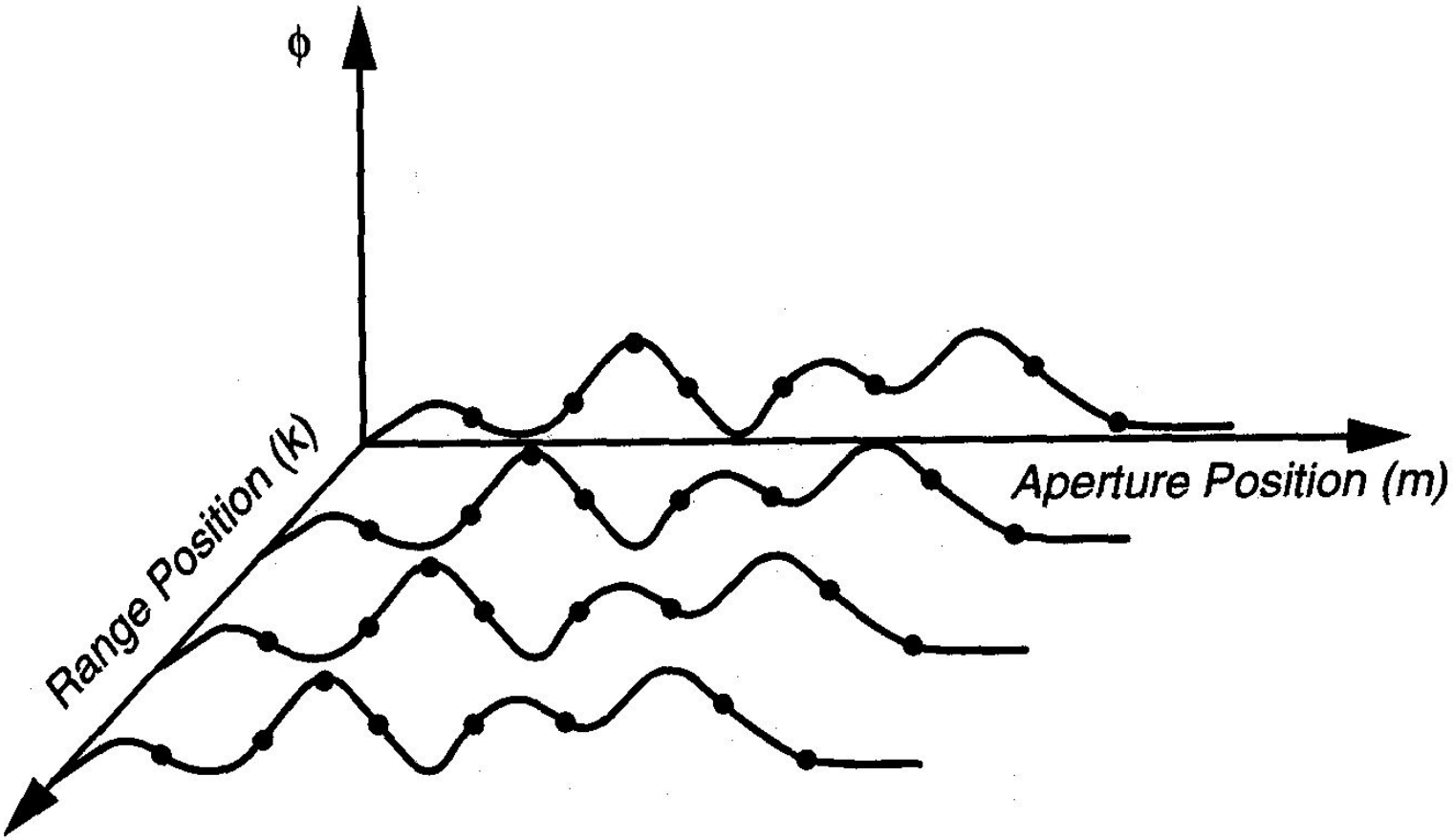

Figure 4.4 Illustration of phase error as a function of aperture position and range in the range-compressed data space. Because the phase function is constant in range, a *slice* in the aperture direction produces the phase-error function.

Motion compensation

In addition to position and attitude knowledge acquired from various external sensors and systems, the radar signal itself can provide information useful in motion compensation.

The Doppler spectrum can be used to detect antenna pointing errors.

The nadir echo can be used to detect vertical velocity (at least over level terrain).

Autofocus

Just as non-ideal motion corrupts the SAR's phase history, the received signal can also reveal the effects of these motion imperfections and subsequently cancel them.

This process is called autofocus.

Various autofocus algorithms are available

- Map drift
- Phase difference
- Inverse filtering
- Phase-gradient autofocus
- Prominent point processing

Many of these techniques exploit the availability of a high-contrast point target in the scene.

Quadratic phase errors

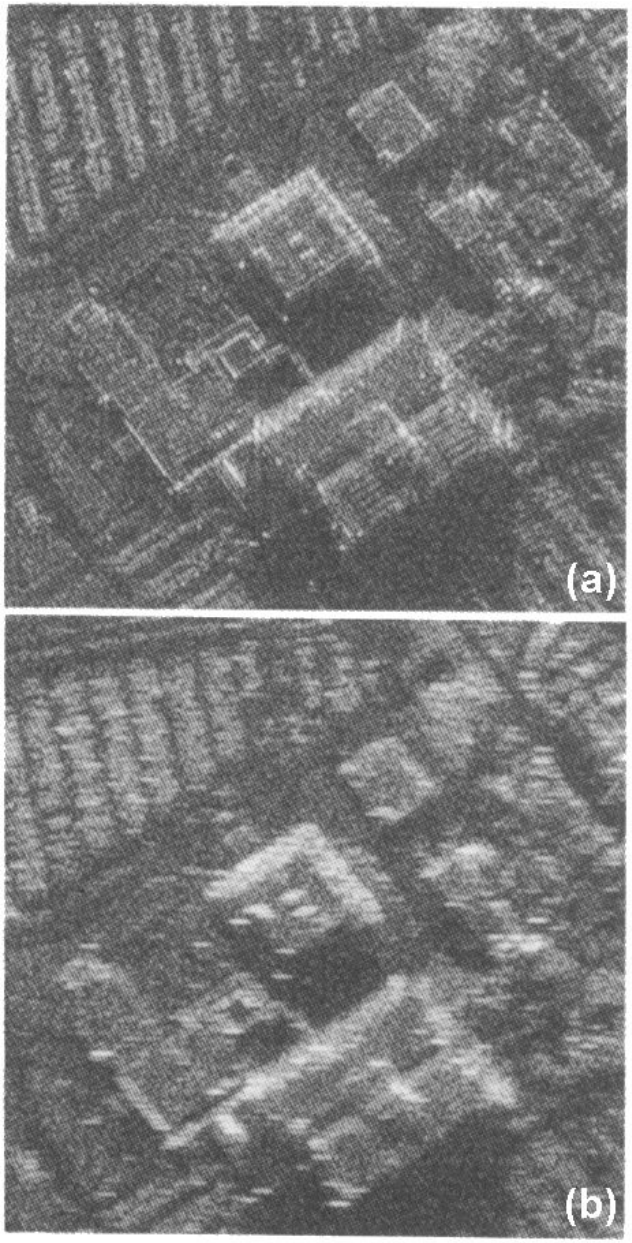

Figure 4.6 SAR image of an urban scene.
(a) Well focused image.
(b) Degraded image caused by a quadratic phase error.

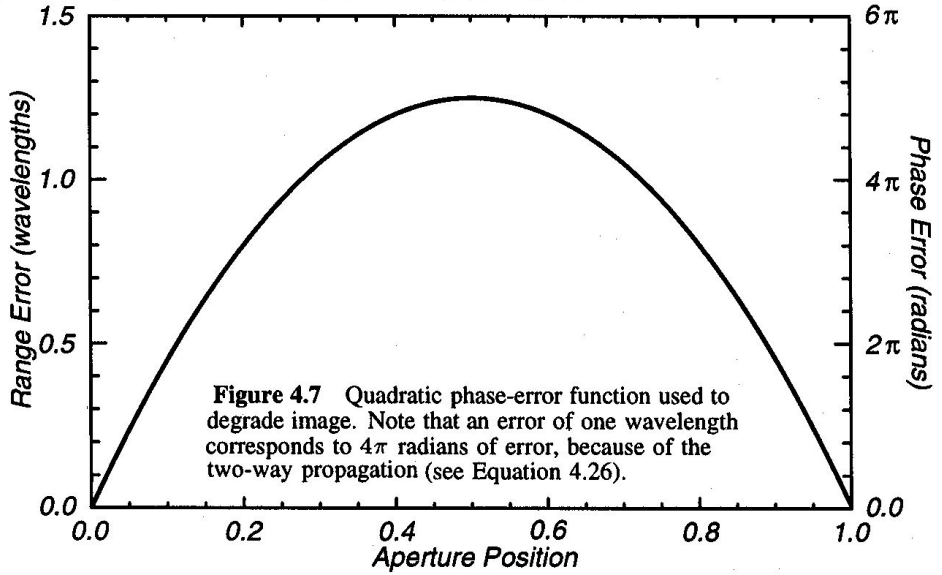

Figure 4.7 Quadratic phase-error function used to degrade image. Note that an error of one wavelength corresponds to 4π radians of error, because of the two-way propagation (see Equation 4.26).

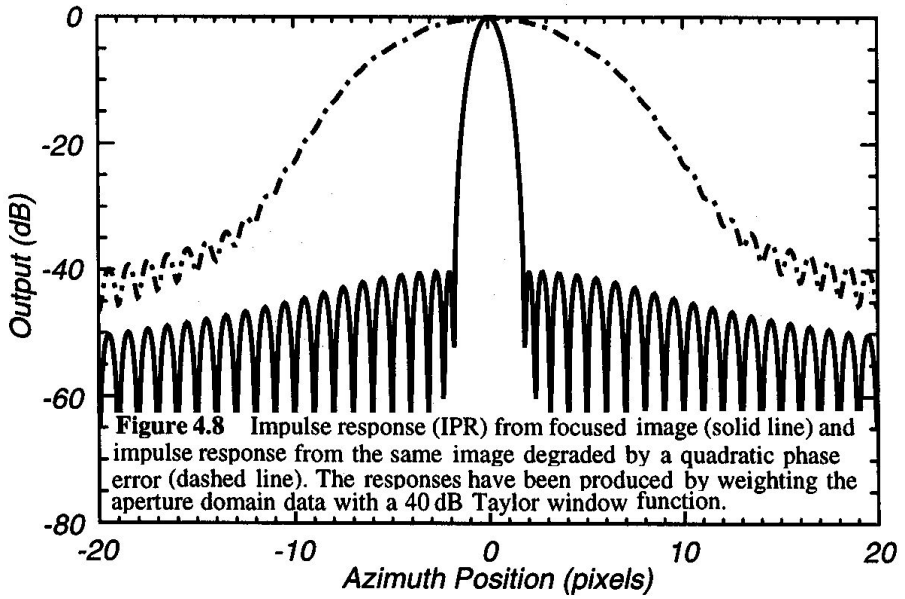

Figure 4.8 Impulse response (IPR) from focused image (solid line) and impulse response from the same image degraded by a quadratic phase error (dashed line). The responses have been produced by weighting the aperture domain data with a 40 dB Taylor window function.

High-frequency phase errors

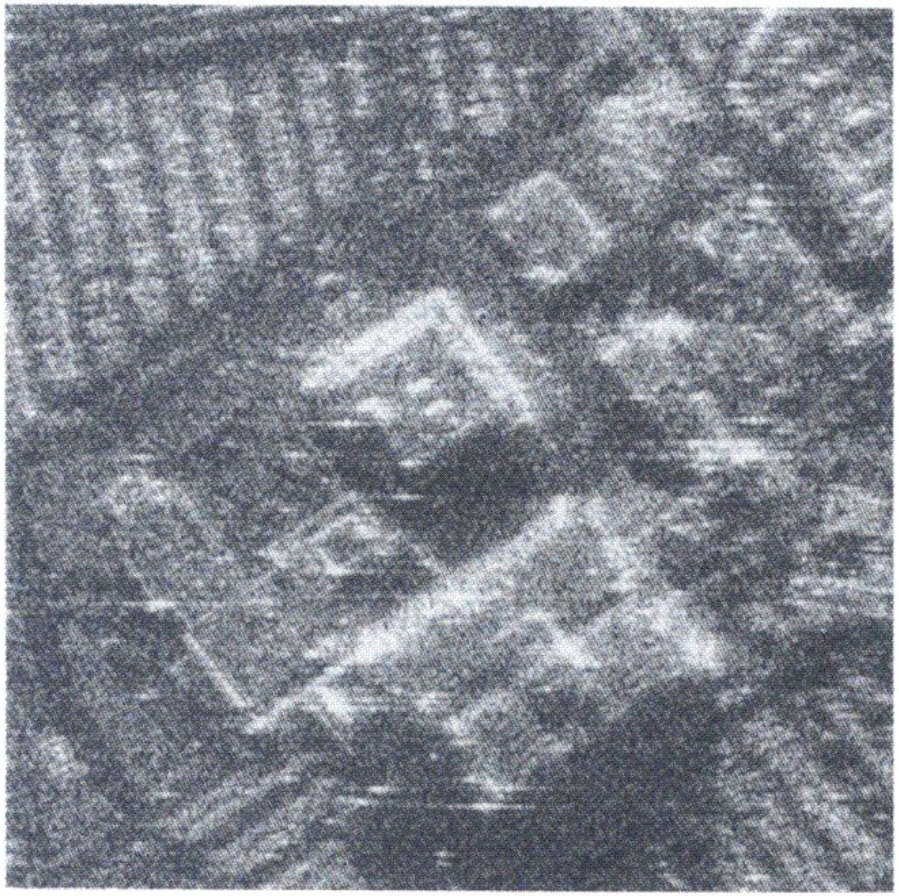

Figure 4.9 Urban SAR scene degraded by a rapidly varying (high frequency) phase error. The peak-to-peak phase variation corresponds to only 1/4 wavelength of relative range error.

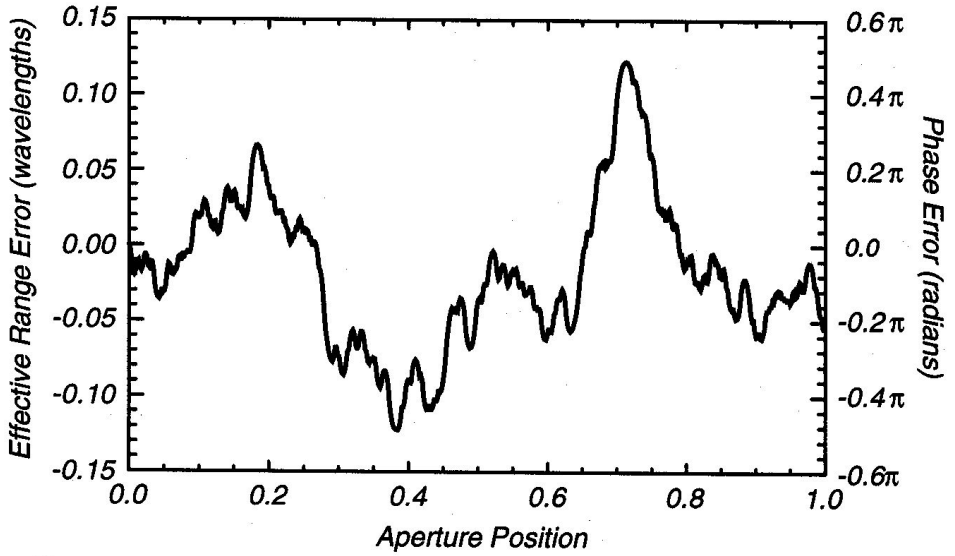

Figure 4.10 Simulated phase error with power-law spectral characteristics. The spectral index used here is $p = 2.5$.

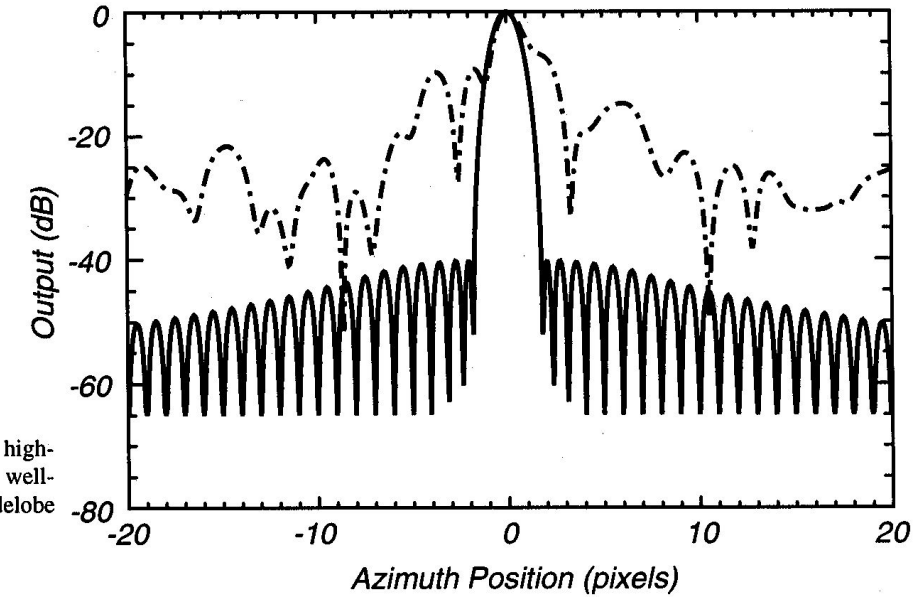

Figure 4.11 Impulse response (dashed line) for the image degraded by the high-frequency (power-law) phase-error function of Figure 4.10. IPR of the original well-focused image is shown by the solid line. Note that the defocus raises the peak sidelobe level by 30 dB in this case.

Autofocus – inverse filtering

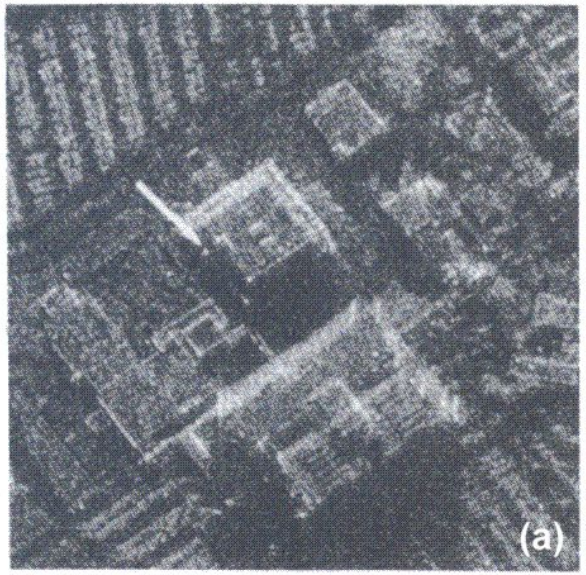

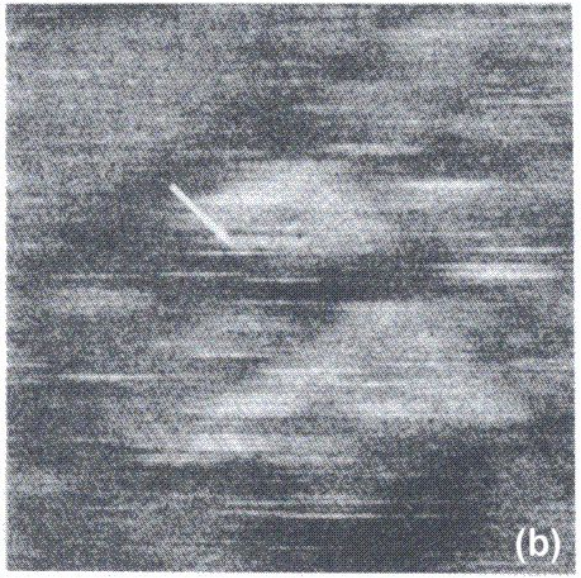

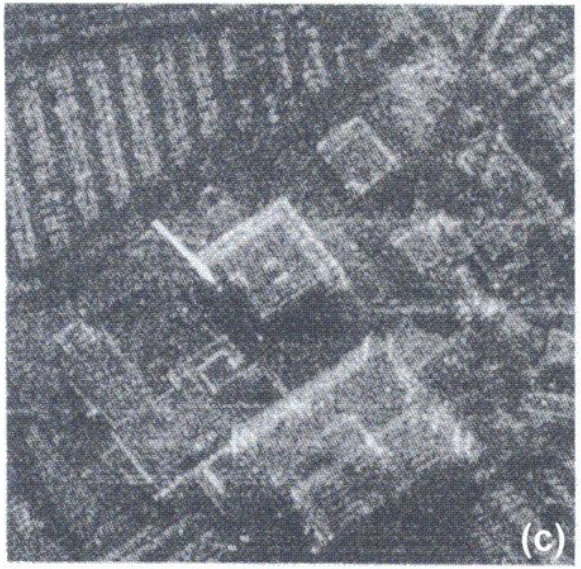

Figure 4.12 Performance of inverse filtering technique for autofocus. SAR images of an urban scene.
(a) Original well-focused SAR image.
(b) Defocused image.
The arrow indicates the target selected to estimate the degrading phase using inverse filtering.
(c) Refocused scene using phase estimated from inverse filtering technique. Residual defocus effects (streaking) are clearly evident.

Aperture Position

Figure 4.13 The original and the estimated low-order phase-error function. The estimated phase error was calculated from the urban scene using the inverse filtering approach. Insert shows residual high-frequency estimation errors that result in streaking effects in refocused image.

Autofocus – inverse filtering

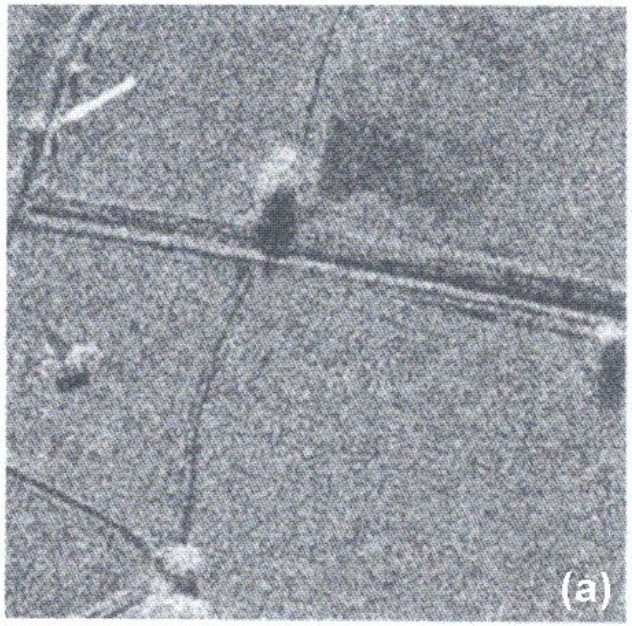

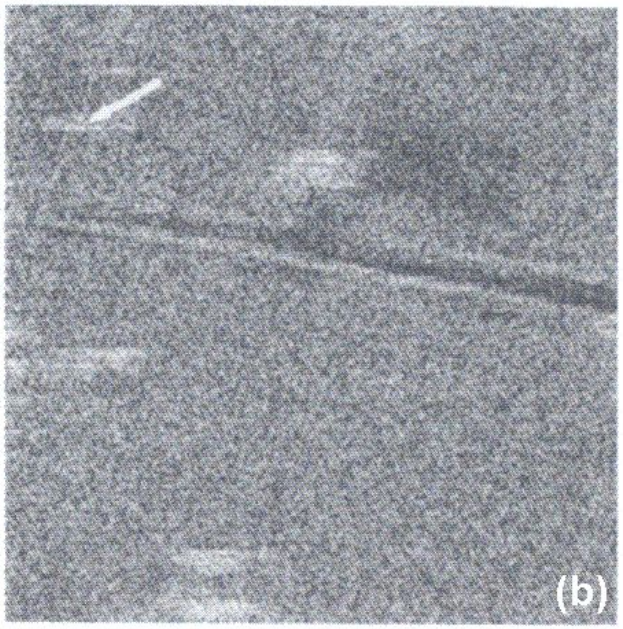

Figure 4.15 SAR images of rural scene
(a) Original well-focused SAR image.
(b) Defocused image.
The arrow indicates the target selected to estimate the degrading phase using inverse filtering.
(c) Focused scene using phase estimated from inverse filtering technique.
Full restoration of the image is clearly not achieved in this case.

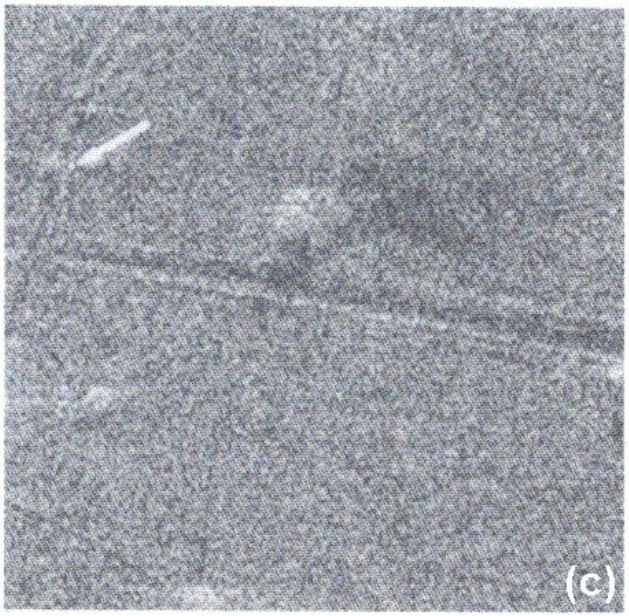

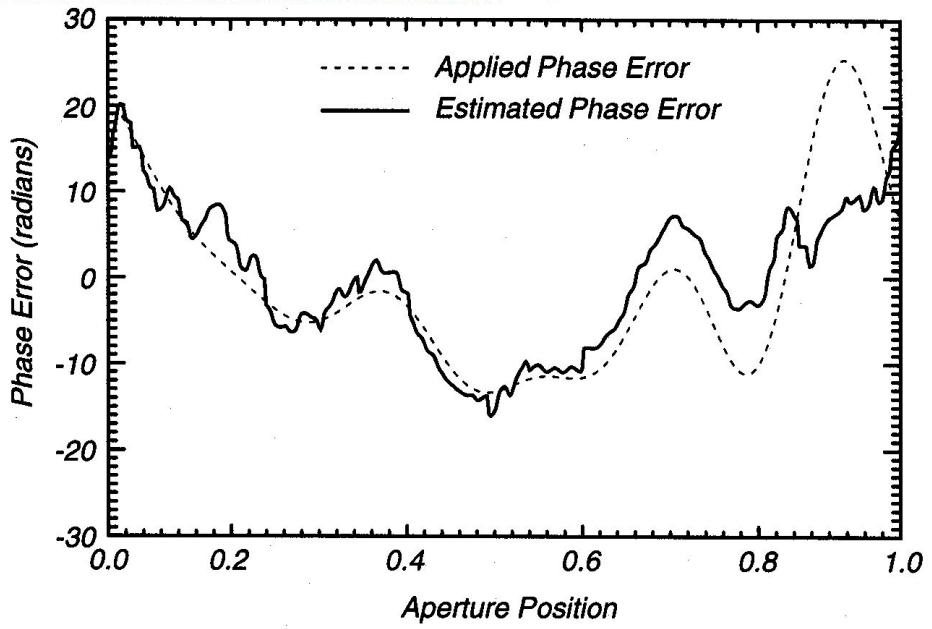

Figure 4.14 The original and estimated phase-error function used on the rural scene. The estimated phase error was calculated using the inverse filtering approach.

Autofocus phase gradient

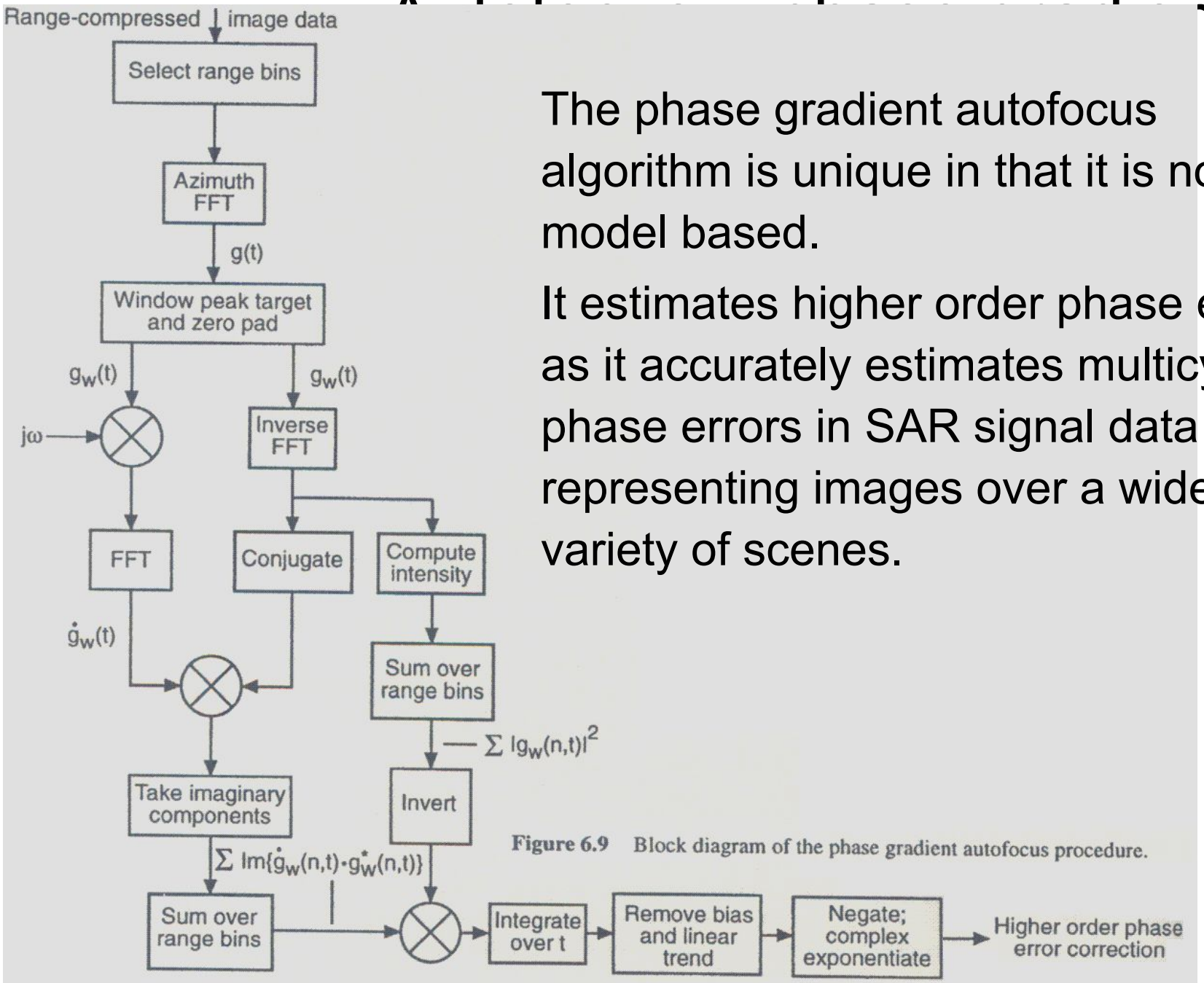

Figure 6.9 Block diagram of the phase gradient autofocus procedure.

The phase gradient autofocus algorithm is unique in that it is not model based.

It estimates higher order phase errors as it accurately estimates multicycle phase errors in SAR signal data representing images over a wide variety of scenes.

Autofocus – phase gradient

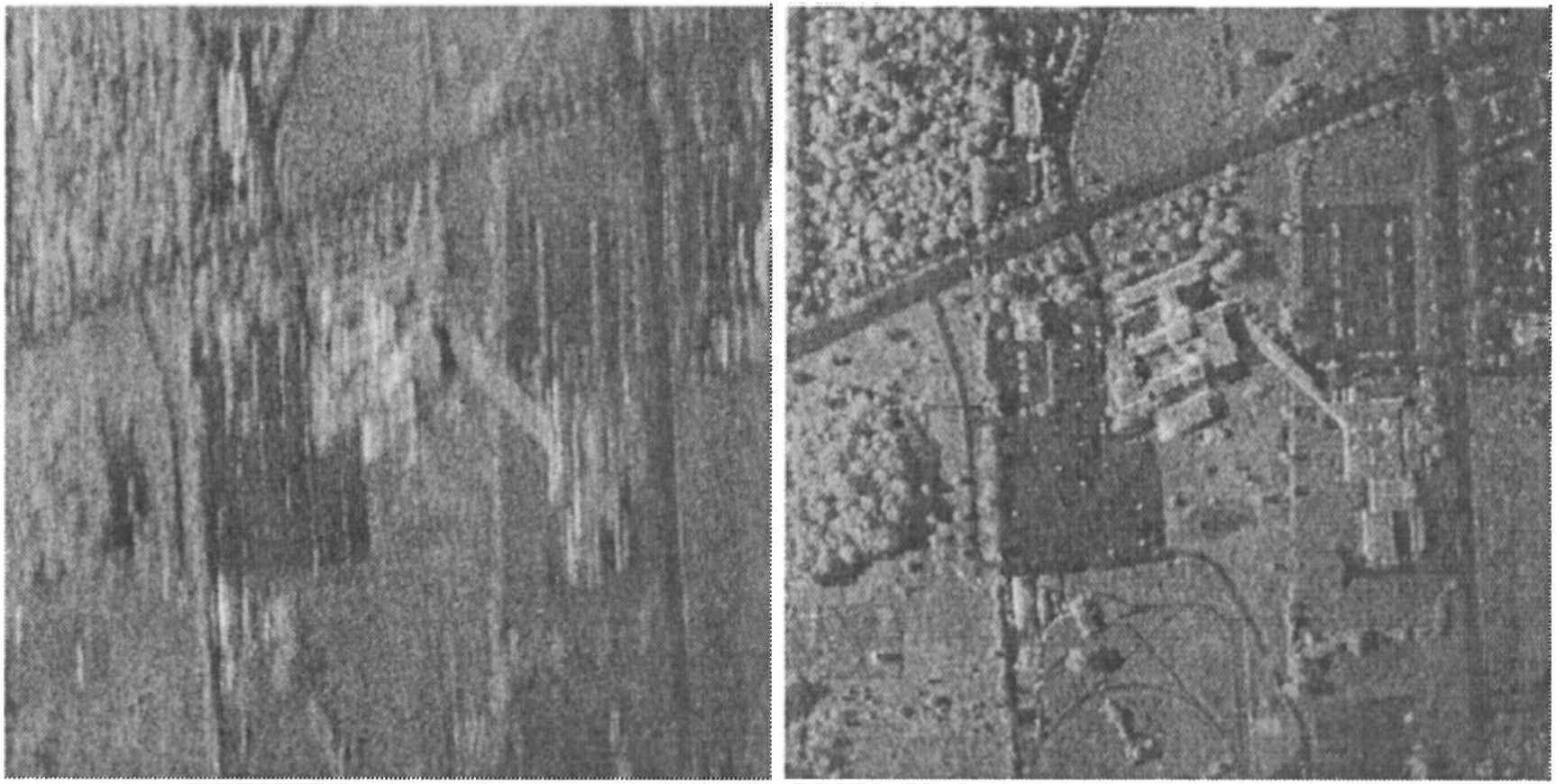

(a) (b)

Figure 6.10 Example of phase gradient autofocus operation: **(a)** Degraded image; **(b)** Image after eight iterations of PGA.